Studies Using Vibrational Sum Frequency Generation Spectroscopy:

I. Salty Glycerol versus Salty Water Surface Organization:

Bromide and Iodide Surface Propensities

II. Influence of Salt Purity on Na^+ and Palmitic Acid Interactions

Thesis

Presented in Partial Fulfillment of the Requirements for the Degree Master of Science in the Graduate School of The Ohio State University

By

Zishuai Huang, B.A.

Graduate Program in Chemistry

The Ohio State University

2013

Thesis Committee:

Heather C. Allen, Advisor

Terry L. Gustafson

Abstract

Salty NaBr and NaI glycerol solution interfaces are examined in the OH stretching region using broadband vibrational sum frequency generation (VSFG) spectroscopy. Raman and infrared (IR) spectroscopy are used to understand further the VSFG spectroscopic signature. The VSFG spectra of salty glycerol solutions reveal that bromide and iodide anions perturb the interfacial glycerol organization in a manner similar as that found in aqueous halide salt solutions, thus confirming the presence of bromide and iodide anions at the glycerol surface. Surface tension measurements are consistent with the surface propensity suggested by the VSFG data and also show that the surface excess increases with increasing salt concentration, similar to that of water. In addition, iodide is shown to have more surface prevalence than bromide, as has also been determined from aqueous solutions. These results suggest that glycerol behaves similarly to water with respect to surface activity and solvation of halide anions at its air/liquid interface.

The influence of salt purity on the interactions between Na^+ ions and the headgroup of palmitic acid (PA) monolayers is studied in the COO^- and OH stretching regions using broadband vibrational sum frequency generation (VSFG) spectroscopy. Ultrapure (UP) and ACS grade NaCl salts are used for aqueous solution preparation after proper pretreatment. The time evolution of VSFG spectra of PA monolayers on solutions made

from these two grades of salts is different, which reveals that the salt purity has a significant impact on the interactions between Na^+ ions and the carboxylate group of PA. The trace metal impurities in ACS grade salt, which are more abundant than in UP grade salt, are responsible for this difference due to their stronger affinity for the carboxylate group relative to Na^+, and further affects the interfacial water structure. These results suggest that the alkali salt grade (after pretreatment) is critical in the studies of alkali cation-carboxylate interactions and comparison of relative binding affinity of different cations.

Dedication

This thesis is dedicated to my parents.

Acknowledgements

I am sincerely grateful to my advisor, Professor Heather C. Allen, for her support, inspiring, encouragement and helpful mentor throughout the last five years. Her meticulousness in research and optimism in life are what I wish to cultivate in my future life. I would also thank Dr. Cheng Y. Tang, Dr. Xiangke Chen and Wei Hua for their great help in both science and life. In addition, I would also extend my thank and best wishes for Dr. Dominique Verreault, Dr. Aaron Jubb and all Allen group members and wish them good luck and success. In the end, I would dedicate my master degree to my family for their education, warm support and encouragement during the past years. I pray sincerely for them for a healthy and happy life every day.

Vita

2008	B.S. Chemistry, Zhejiang University, China
2008 to 2010	Graduate Teaching Associate, Department of Chemistry and Biochemistry, The Ohio State University
2010 to present	Graduate Researching Associate, Department of Chemistry and Biochemistry, The Ohio State University

Publications

- X. Chen, W. Hua, Z. Huang, H. C. Allen; Interfacial Water Structure Associated with Phospholipid Membranes Studied by Phase-Sensitive Vibrational Sum Frequency Generation Spectroscopy, ***J. Am. Chem. Soc.*** 132(32), 11336-11342 (2010).
- C. Y. Tang, Z. Huang, H. C. Allen; Binding of Mg^{2+} and Ca^{2+} to Palmitic Acid and Deprotonation of the COOH Headgroup Studied by Vibrational Sum Frequency Generation Spectroscopy, ***J. Phys. Chem. B*** 114(51), 17068-17076 (2010).

- X. Chen, W. Hua, Z. Huang, H. C. Allen; Reorganization and Caging of DPPC, DPPE, DPPG, and DPPS Monolayers Caused by Dimethylsulfoxide Observed Using Brewster Angle Microscopy, ***Langmuir*** 26(24), 18902-18908 (2010).
- C. Y. Tang, Z. Huang, H. C. Allen; Interfacial Water Structure and Effects of Mg^{2+} and Ca^{2+} Binding to the COOH Headgroup of Palmitic Acid Monolayer Studied by Vibrational Sum Frequency Generation Spectroscopy, ***J. Phys. Chem. B*** 115(1), 34-40 (2011).
- A. G. F. de Beer, J. S. Samson, W. Hua, Z. Huang, X. Chen, H. C. Allen, S. Roke; Direct comparison of Phase-Sensitive Vibrational Sum Frequency Generation with Maximum Entropy Method: Case Study of Water, ***J. Chem. Phys.*** 135(22), 224701/1-224701/9 (2011).
- Z. Huang, W. Hua, D. Verreault, H. C. Allen; Salty Glycerol Versus Salty Water Surface Organization: Bromide and Iodide Surface Propensities, ***J. Phys. Chem. A***, *Articles ASAP* (2013).

Fields of Study

Major Field: Chemistry.

Table of Contents

List of Tables

List of Figures

Chapter 1: Introduction

Interfaces in nature are of great importance due to their ubiquity in biology and environment and understanding of interfacial structures is essential in modern chemistry. Gas-liquid interactions are prevalent in atmospheric and biological chemistry.[1] Gas phase molecules coming into contact and interacting with liquids have been studied to understand the fundamentals in the reactions between gases and liquids.[1-5] Further, the solvation of ions at interfaces is involved in many chemical, biological and atmospheric processes and is believed to be able to change the fate of reactions at the surfaces.[4,5] Glycerol shares some physical properties with water such as an extensive hydrogen bonding network, high surface tension (water: ~72.8 mN/m, glycerol: ~63.4 mN/m at 293 K),[6,7] and a large dielectric constant (water: ~80.2, glycerol: 41.1 at 293 K).[6,8] As a promising proxy for water in research, it is relevant to examine similarities and differences between these two important solvents. This thesis presents studies of interfaces of air/glycerol and air/glycerol solutions of halide salts in comparison with air/water and air/water solutions of halide salts.

On the other hand, surfactants at air/water interface have attracted much attention as they are closely relevant to the biological membranes and marine aerosols. Cation-specific effects on the surfactants in aqueous solutions are essential to many chemical biochemical and atmospheric processes.[9-16] Particularly, sodium and potassium, as the two

most abundant alkali cations in intra- and extracellular fluids, play a critical role in electrical communication across cell membranes.[17-19] The interaction between alkali cations and carboxylate groups have been extensively studied.[16,20-29] The above experimental results related to Na^+ and K^+[13,20,25,28] suggested that Na^+ has stronger binding affinity to COO^- relative to K^+. In contrast, Tang and Allen, by using VSFG spectroscopy, pointed out a greater affinity of K^+ than Na^+ to the COO^- in palmitic acid.[16] Different grades of salt and the trace amount of polyvalent cations in salts may be responsible for the controversy. In this thesis, the influence of salt purity on the interaction between Na^+ and PA headgroup is studied in COO^- and OH stretching regions.

Chapter 2 gives a brief introduction of the VSFG theory and Chapter 3 describes the VSFG instruments used in this work.

Chapter 4 reports the conventional VSFG, Raman and IR spectra along with preliminary phase-sensitive VSFG and surface pressure data of glycerol and halide salt glycerol solutions. The halide salts are found to be present at the air/glycerol interface and perturb the glycerol hydrogen bonding network. The more polarizable I^- has a larger impact on the hydrogen bonds than Br^-. The phase-sensitive VSFG data show that Br^- and I^- can reorient the OH groups in glycerol molecules. Moreover, surface tension measurements suggest a similar trend in surface excess of halide anions to the air/glycerol and air/water interfaces.

Chapter 5 reports the VSFG spectra of PA monolayers on 0.6 M UP grade and ACS grade NaCl solutions in COO^- and OH stretching regions. The evolution of VSFG spectra

of PA monolayer on solutions of these two grades of salts is different, which reveals that the salt purity has a significant impact on the interaction between Na^+ and carboxylate group. The trace metal impurities in ACS grade salt, which is much higher than in UP grade salt, is responsible for this difference due to their stronger affinity relative to Na^+, and further affects the interfacial water structure.

Chapter 2: Theory

2.1. Sum Frequency Generation (SFG) Theory

The detailed descriptions of the second-order optical processes are presented in literature. Here only a brief introduction is given in this section. Sum frequency generation is second order nonlinear optical phenomenon in the event of intense optical radiations. High power coherent light source such as lasers is necessary for this process. Vibrational sum frequency generation (VSFG) spectroscopy is a surface specific technique that is widely used to investigate molecular structures and orientations at surface or interface. The VSFG process is driven by two pulsed laser beams, one visible (ω_{vis}) and the other infrared (ω_{IR}). The IR beam is often tunable in a broad range such that it can cover all the vibrational regions of interest. These two beams are overlapped at a surface or an interface both spatially and temporally to generate a third beam that has a frequency $\omega_{SF} = \omega_{vis} + \omega_{IR}$.

The intensity of the sum frequency signal I_{SF} is proportional to the absolute square of the second-order susceptibility $\chi_{eff}^{(2)}$ and to the visible and IR beam intensities:

$$I_{SF} = \frac{8\pi^3 {\omega_{SF}}^2 \sec^2\theta_{SF}}{c^3 n_1(\omega_{SF}) n_1(\omega_{vis}) n_1(\omega_{IR})} \left|{\chi_{eff}}^{(2)}\right|^2 I_{vis} I_{IR} \tag{2-1}$$

with

$$\chi_{eff}^{(2)} = [L(\omega_{SF}) \cdot \hat{e}(\omega_{SF})] \cdot \chi^{(2)} : [L(\omega_{vis}) \cdot \hat{e}(\omega_{vis})] \cdot [L(\omega_{IR}) \cdot \hat{e}(\omega_{IR})] \quad (2\text{-}2)$$

where ω_i is the frequency of visible, IR and sum frequency beams, $n_1(\omega)$ is the refractive index of the medium where the beams are incident and reflected to at frequency ω. The effective second-order susceptibility $\chi_{eff}^{(2)}$ is related to the macroscopic second-order susceptibility $\chi^{(2)}$ by the Fresnel factors $L(\omega)$ and the unit electric field vector $\hat{e}(\omega)$.

$\chi^{(2)}$ is the macroscopic average of the molecular hyperpolarizabilities $\beta^{(2)}$ of the molecules adsorbed at the interface. As ω_{IR} is tuned through a vibrational resonance, the values of β^2 change and so as $\chi^{(2)}$ and the SF signal intensity is resultantly changed. β^2 has a total of 27 components that describe the non-linear response of the molecule to all incident and emitted electric field polarization combinations. Similarly, the non-linear susceptibility $\chi^{(2)}$ also has a maximum of 27 components. However, not all components contribute to the value of $\chi^{(2)}$ due to the symmetry constraints. In a centrosymmetric environment, bulk solution for example, all directions are equivalent and the value of $\chi_{ijk}^{(2)}$ for two opposing directions should be identical:

$$\chi_{ijk}^{(2)} = \chi_{-i-j-k}^{(2)} \quad (2\text{-}3)$$

However, $\chi_{ijk}^{(2)}$ as a third rank tensor, a change in the sign of the three subscripts is simply equivalent to reversing the axis system, and therefore reverse the sign of $\chi_{ijk}^{(2)}$:

$$\chi_{ijk}^{(2)} = -\chi_{-i-j-k}^{(2)} \quad (2\text{-}4)$$

To satisfy both equation (2-3) and (2-4), $\chi_{ijk}^{(2)}$ must equal 0, indicating that there is no SFG response in a centrosymmetric medium such as bulk phases. In contrast, the boundary between two media is lacking of the centrosymmetry and is therefore SFG active.

If an isotropic interface is defined as a *xy* plane and *z* axis is perpendicular to the interface, there are only 7 non-vanishing components among the total 27 components. Since the x and y axes are equivalent for an isotropic surface, there are in fact four independent non-zero $\chi_{ijk}^{(2)}$ components that can potentially generate a SFG signal:

$$\chi_{zxx}^{(2)}\left(\equiv \chi_{zyy}^{(2)}\right)\ \ \chi_{xzx}^{(2)}\left(\equiv \chi_{yzy}^{(2)}\right)\ \ \chi_{xxz}^{(2)}\left(\equiv \chi_{yyz}^{(2)}\right)\ \ \chi_{zzz}^{(2)}$$

By choosing different polarization combinations of the incident visible, IR and generated SFG beams, each $\chi_{ijk}^{(2)}$ can be experimentally determined. In practice, *ssp* polarization denotes the polarizations of the SFG, visible and IR to be *s*, *s* and *p*, respectively. $\chi_{eff}^{(2)}$ is a linear combination of the macroscopic $\chi_{ijk}^{(2)}$ and shown as following:

$$\chi_{eff,ssp}^{(2)} = L_{yy}(\omega_{SF})L_{yy}(\omega_{vis})L_{zz}(\omega_{IR})\sin\theta_{IR}\,\chi_{yyz}$$

$$\chi_{eff,sps}^{(2)} = L_{yy}(\omega_{SF})L_{zz}(\omega_{vis})L_{yy}(\omega_{IR})\sin\theta_{vis}\,\chi_{yzy}$$

$$\chi_{eff,pss}^{(2)} = L_{zz}(\omega_{SF})L_{yy}(\omega_{vis})L_{yy}(\omega_{IR})\sin\theta_{SF}\,\chi_{zyy}$$

$$\chi_{eff,ppp}^{(2)} = -L_{xx}(\omega_{SF})L_{xx}(\omega_{vis})L_{zz}(\omega_{IR})\cos\theta_{SF}\cos\theta_{vis}\sin\theta_{IR}\,\chi_{xxz}$$

$$-L_{xx}(\omega_{SF})L_{zz}(\omega_{vis})L_{xx}(\omega_{IR})\cos\theta_{SF}\sin\theta_{vis}\cos\theta_{IR}\,\chi_{xzx}$$

$$+L_{zz}(\omega_{SF})L_{xx}(\omega_{vis})L_{xx}(\omega_{IR})\sin\theta_{SF}\cos\theta_{vis}\cos\theta_{IR}\,\chi_{zxx}$$

$$+L_{zz}(\omega_{SF})L_{zz}(\omega_{vis})L_{zz}(\omega_{IR})\sin\theta_{SF}\sin\theta_{vis}\sin\theta_{IR}\,\chi_{zzz} \quad (2\text{-}5)$$

As mentioned above, $\chi^{(2)}$ is the macroscopic average of microscopic hyperpolarizability $\beta^{(2)}$ and related through:

$$\chi^{(2)} = N_S\langle\beta^{(2)}\rangle \quad (2\text{-}6)$$

with $\beta^{(2)}$ given by the product of the Raman transition polarizability moment (α) and the IR transition dipole moment (μ)

$$\beta^{(2)} = \langle g|\alpha|v\rangle\langle v|\mu|g\rangle \quad (2\text{-}7)$$

where N_S is the number of molecules contributing to the SFG signal and g and v are the ground and excited vibrational states, respectively. Equation (2-6) and (2-7) state that to be VSFG responsive, a vibrational mode must be both IR and Raman active.

VSFG intensity can be also related to a vibrational mode via following equations:

$$I_{SF} \propto \left|\chi^{(2)}_{eff}\right|^2 I_{vis}I_{IR} \quad (2\text{-}8)$$

$$\chi^{(2)}_{eff} = [L(\omega_{SF})\cdot\hat{e}(\omega_{SF})]\cdot\chi^{(2)} : [L(\omega_{vis})\cdot\hat{e}(\omega_{vis})]\cdot[L(\omega_{IR})\cdot\hat{e}(\omega_{IR})] \quad (2\text{-}2)$$

$$\chi^{(2)} = \chi^{(2)}_{NR} + \sum_v \chi^{(2)}_v \quad (2\text{-}9)$$

$$\chi^{(2)}_v = \frac{A_v}{\omega_{IR}-\omega_v+i\Gamma_v} \quad (2\text{-}10)$$

where the macroscopic second-order nonlinear susceptibility $\chi^{(2)}$ consists of resonant terms $\chi^{(2)}_v$ and a nonresonant term $\chi^{(2)}_{NR}$, A_v is the amplitude of the transition moment, and

Γ_v is the width of the vibrational transition, also known as the half-width at half-maximum (hwhm). Equation (2-2) and (2-8) through (2-10) indicate that the VSFG intensity is optimally enhanced when the frequency of incident IR beam equal to a specific vibrational mode.

2.2. Phase-sensitive Vibrational Sum Frequency Generation (PS-VSFG) Theory

However, conventional VSFG fails to determine the sign of $\chi^{(2)}$ as well as to differentiate the resonant real part of $\chi^{(2)}$ (Re$\chi^{(2)}$), the imaginary part of $\chi^{(2)}$ (Im$\chi^{(2)}$) and the nonresonant term $\chi_{NR}^{(2)}$. Phase-sensitive vibrational sum frequency generation can reveal the sign of $\chi^{(2)}$ and provide orientational information of vibrations compared to conventional VSFG. In this thesis, the term VSFG refers to conventional VSFG in contrast with PS-VSFG.

Although the nonresonant term is negligible compared to the resonant terms for air/water interface, the overlapping vibrational modes makes the fitting of peaks extremely difficult and the fitting parameters obtained from VSFG spectra are not unique if the phase information of each mode is unknown.[30] A small change in phase may cause a completely different peak assignment. $\chi^{(2)}$ is a complex number in a form of:

$$\chi^{(2)} = \left|\chi^{(2)}\right| e^{i\phi(\omega_{IR})} = Re\chi^{(2)} + i\, Im\chi^{(2)} \tag{2-11}$$

where $\left|\chi^{(2)}\right|$ and ϕ are the amplitude and phase of $\chi^{(2)}$, respectively. Combining equation (2-9) and (2-10), the imaginary part of $\chi^{(2)}$ is derived as:

$$Im\chi^{(2)} = -\sum_v \frac{A_v \Gamma_v}{(\omega_{IR}-\omega_v)^2+\Gamma_v^2} \quad (2\text{-}12)$$

In order to obtain the phase information experimentally, PS-VSFG utilizes an additional signal called local oscillator which is generated from a nonresonant nonlinear crystal GaAs and coupled with the SFG signal from sample. This technique was first pioneered by Shen and coworkers.[30,31] Recently PS-VSFG research has been conducted by more groups, including Stiopkin et al.[32], Tahara and coworkers,[33] and Allen and coworkers.[34,35]

The instrumental setup in our lab is similar as reported by Nihonyanagi et al. The SFG signal of sample interferes with a local oscillator delayed by ΔT by a silica plate. The expression of the detected total SFG signal is therefore a mixture of two terms:

$$E_{total}(t) = E_{sample}(t-\Delta T) + E_{LO}(t) \quad (2\text{-}13)$$

Applying Fourier transform to equation (2-13) gives:

$$E_{total}(\omega) = \int_{-\infty}^{+\infty} dt E_{total}(t) e^{i\omega t} = E_{sample}(\omega) e^{i\omega\Delta T} + E_{LO}(\omega) \quad (2\text{-}14)$$

The detected VSFG intensity is:

$$I_{SF} \propto |E_{total}|^2 = \left|E_{sample}\right|^2 + |E_{LO}|^2 + E_{sample} {E_{LO}}^* e^{i\omega\Delta T} + {E_{sample}}^* E_{LO} e^{-i\omega\Delta T} \quad (2\text{-}15)$$

Equation (2-15) clearly shows that the interference between the sample SFG and local oscillator is buried in the cross terms and the phase information is preserved. In the time domain, the first two terms in equation (2-15) are located at 0, and the cross terms are separated at positive and negative axes, ΔT relative to the origin. The two cross terms are

equivalent and only one is sufficient for data process. After filtration of the three terms, the remaining cross term is then Fourier transformed to the frequency domain.

The sum frequency electric fields of sample and reference are E_{sample} and E_{ref}, respectively. Their corresponding local oscillator electric fields are$E_{LO,s}$ and $E_{LO,r}$. They can be expressed using the second-order nonlinear susceptibilities of the sample and reference ($\chi^{(2)}_{sample}$, $\chi^{(2)}_{ref}$):[36]

$$E_{sample} = ia_{sample}\chi^{(2)}_{sample}E_{vis}E_{IR} \tag{2-16}$$

$$E_{LO,s} = a_{LO}\chi^{(2)}_{LO}r^{s}_{vis}E_{vis}r^{s}_{IR}E_{IR} \tag{2-17}$$

$$E_{ref} = a_{ref}\chi^{(2)}_{ref}E_{vis}E_{IR} \tag{2-18}$$

$$E_{LO,r} = a_{LO}\chi^{(2)}_{LO}r^{r}_{vis}E_{vis}r^{r}_{IR}E_{IR} \tag{2-19}$$

where a_{sample}, a_{ref} and a_{LO} are real and positive constants and r^{i}_{vis} and r^{i}_{IR} are the reflectivities of the medium *i* for E_{vis} and E_{IR}. For instance, since quartz does not have any resonance in the infrared region, the phase of z-cut quartz can be used as a reference (φ_{ref}). By dividing the sample interferogram by the reference interferogram, the real and imaginary parts of $\chi^{(2)}$ as well as the spectra normalized to the reflectivities can be obtained. The normalized PS-VSFG spectrum is:

$$I_{PS} = \frac{a_{sample}r^{s}_{vis}r^{s}_{IR}}{a_{\,ref}r^{r}_{vis}r^{r}_{IR}}\frac{\chi^{(2)}_{sample}}{\chi^{(2)}_{ref}} \tag{2-20}$$

The $Im\chi^{(2)}$ spectrum is:

$$Im\chi^{(2)} \propto \frac{r_{vis}^{r} r_{IR}^{r} |E_{sample} E_{LO}|}{r_{vis}^{s} r_{IR}^{s} |E_{ref} E_{LO}|} \sin(\varphi_{sample} - \varphi_{ref}) \quad (2\text{-}21)$$

Particularly, in water OH stretch region, the macroscopic second-order susceptibility $\chi^{(2)}$ for the water OH symmetric stretch is:[33]

$$\chi_{yyz}^{OH,ss} = \frac{1}{2} N_S \beta_{ccc} \left\{ \left(1.296 + 0.557 \frac{\langle \cos^3 \theta \rangle}{\langle \cos \theta \rangle}\right) \langle \cos^2 \psi \rangle + \left(0.557 + 1.296 \frac{\langle \cos^3 \theta \rangle}{\langle \cos \theta \rangle}\right) \langle \sin^2 \psi \rangle + \left(1 - \frac{\langle \cos^3 \theta \rangle}{\langle \cos \theta \rangle}\right) \right\} \langle \cos \theta \rangle \quad (2\text{-}22)$$

where θ is the tilt angle between water dipole and the outwards surface normal, ψ is the twist angle. When $0° < \theta < 90°$, $\cos\theta > 0$, $\chi_{yyz}^{OH,ss}$ is positive. This indicates that if the $Im\chi^{(2)}$ is positive the water dipoles are orienting towards the air phase, or the OH group is pointing upwards to the air, and vice versa.

Chapter 3: Instrumentation

3.1. Conventional Broad Bandwidth Sum Frequency Generation Instrumentation

VSFG spectroscopy measurements were performed using a broadband VSFG spectrometer setup that has been described elsewhere.[16,37-39] Briefly, a titanium:sapphire oscillator (Tsunami, Spectra-Physics) with a center wavelength at 800 nm was used to seed two 1 kHz regenerative amplifiers (Spitfire femtosecond and picosecond versions, Spectra-Physics) that are pumped by a solid-state Nd:YLF laser (Evolution 30, SpectraPhysics) at 527 nm. The amplifiers generate narrowband (2 ps, ~17 cm^{-1} bandwidth, >0.9 W) and broadband (~85 fs, ~345 cm^{-1} bandwidth, ~1 W) laser pulses at 800 nm.[39] The narrow-bandwidth beam was used as the visible beam, while the broad-bandwidth beam was further directed to an optical parametric amplifier (TOPAS-C, Light Conversion) coupled to a narrow-difference frequency generation system (NDFG, Light Conversion) that generated a tunable mid-IR beam. The full spectral bandwidth of the generated broadband IR beam was ~800 cm^{-1} in the OH stretching region (3000-3800 cm^{-1}) and ~250 cm^{-1} in the COO^- stretching region (1350-1600 cm^{-1}). The spectral resolution is ~8 cm^{-1}. The average energies of the IR beams for the OH and COO^- stretching region were ~10 μJ and ~6 μJ, respectively. The average energy of the visible beams for both region was 300 μJ.

Furthermore, the setup was purged with dry nitrogen to minimize the energy loss from the absorption of water vapor in the air.

The visible (*s*-polarized) and IR (*p*-polarized) beams are spatially and temporally overlapped on the sample's surface (including GaAs) to generate a sum-frequency (SF) beam (*s*-polarized) (Figure 3.1). In Chapter 4, the copropagating visible and IR beams impinge on the sample surface at incident angles of 59° and 63°, respectively. In Chapter 5, the incident angles of visible and IR beams are of 53° and 68°, respectively. The reflected SF beam was then dispersed by a monochromator (SpectraPro SP-500, Acton Research; 1200 g/mm grating blazed at 750 nm) and detected by a liquid-nitrogen-cooled charge-coupled device (CCD) camera (Spec-10:400B: LN400EB back-illuminated, Roper Scientific; 1340 × 400 pixel array). The noise that can contribute to the VSFG spectrum background was subtracted by adjusting the time delay and re-measuring the VSFG background spectrum. (Glycerol is highly viscous and the surface generates more scattering relative to neat water upon the illumination of the pulsed light, and thus contributes to the noise in the spectrum.) The background-subtracted VSFG spectra were normalized to the broadband infrared beam energy profile using a non-resonant VSFG spectrum from a GaAs crystal (Lambda Precision Optics, Inc.). The purpose of doing the normalization is to eliminate the spectral distortion caused by the infrared beam energy distribution associated with each frequency in the spectral region of interest. The VSFG spectral calibration was accomplished by measuring the absorption of polystyrene in the IR profile obtained from the GaAs spectrum. In the glycerol experiment, two spectra were

averaged for each sample and the acquisition time for each spectrum was set to 5 min. All spectra were obtained at room temperature.

For the studies presented here it is important to note that VSFG probes the interface where there is lack of symmetry of inversion at a maximum depth that is approximately half the shortest wavelength. However, this is dependent on the chemical system and in some cases the probe depth can be as small as 1-5 nm as in neat water.

3.2. Broad Bandwidth Phase-sensitive Sum Frequency Generation Instrumentation

The instrumental setup of our broad bandwidth phase-sensitive sum frequency generation is identical with the conventional VSFG setup in most parts and shown elsewhere.[34] A narrow broad visible beam (2 ps, ~17 cm^{-1} bandwidth, >0.9 W) and a broad band IR beam (~85 fs, ~345 cm^{-1} bandwidth, ~1 W) are spatially and temporally overlapped at the sample surface on the first sample stage, generating a reflected SFG signal. This SFG signal is time delayed by a silica plate by (1.7-2.6 ps) and then refocused along with the reflected visible and IR beams by a gold concave mirror (f = 100 mm) onto a GaAs crystal on a second sample stage. The SFG signal generated at GaAs interferes with the first SFG signal and the interferogram is stretched in a monochromator (SpectraPro SP-500, Acton Research; 1200 g/mm grating blazed at 750 nm) and detected in a liquid-nitrogen cooled charge-coupled device (CCD) camera (Spec-10:400B: LN400EB back-illuminated, Roper Scientific; 1340 × 400 pixel array).The height of the sample surface is extremely critical and a very small variation has a great impact on the

final spectra. To minimize the error, the height is regularly checked and kept unchanged by observing the pixel number where the obtained image is located. Final spectra are processed from the raw interferograms through Fourier transformation.

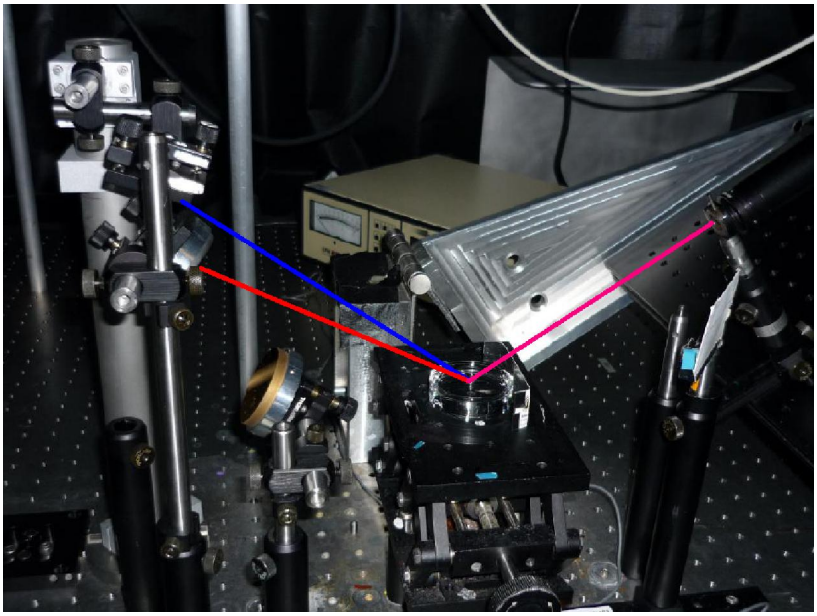

Figure 3.1. Conventional VSFG setup configuration at the sample stage.

Chapter 4: Salty Glycerol versus Salty Water Surface Organization: Bromide and Iodide Surface Propensities

4.1. Introduction

Glycerol is a colorless, low toxicity, viscous liquid polyol with three hydroxyl groups, which is moderately hygroscopic and completely miscible with water.[6,40] It also serves as a good protic solvent for many inorganic and organic compounds due to its amphiphilic nature. In part due to its low toxicity, it has a wide range of applications including, among others, its uses as an antifreeze and cryoprotecting agent, as a detergent, as well as a moisturizing and lubricating agent in cosmetics and pharmaceutical products.[41] Despite its viscous nature, glycerol shares some physical properties with water such as an extensive hydrogen bonding network, high surface tension (water: ~72.8 mN/m, glycerol: ~63.4 mN/m at 293 K),[6,7] and a large dielectric constant (water: ~80.2, glycerol: 41.1 at 293 K).[6,8] Therefore, as a promising proxy for water in research, it is relevant to examine similarities and differences between these two important solvents.

Some work has been done on pure glycerol to explore its bulk and interfacial structures. Champeney et al. studied deuterated glycerol using neutron diffraction in the bulk liquid and proposed that the glycerol structure is highly dependent on hydrogen bonding with neighboring molecules and that all molecules are likely to be interlinked by

a sequence of hydrogen bonds.[42] Root and Stillinger using molecular dynamics (MD) simulations obtained a monomer isomer with an extended conformation similar to that found in glycerol crystal.[43] Chelli et al. also studied glycerol condensed phase by MD simulations and focused on the conformational structure and hydrogen bonding.[44] Soltwisch and Steffen concluded from their X-ray scattering experiments that glycerol crystalline conformation is probably predominant in the liquid phase.[45] Different groups using spectroscopic methods such as Raman,[46,47] attenuated total reflection infrared (ATR-IR),[47,48] vibrational sum frequency generation (VSFG) spectroscopy,[49,50] and electron energy loss spectroscopy[51] showed that, both in the bulk and at the interface, pure glycerol exhibits a broad OH stretching band from 3000-3600 cm^{-1} characteristic of hydrogen-bonded glycerol molecules. Yet, unlike water, no dangling OH stretch was observed for the pure glycerol surface.[49,50]

With respect to the ion-solvent system, only a few reports about the solvation of ions in glycerol are available.[52,53] Yet there has been some interest around glycerol surfaces and ion solvation. Nathanson and coworkers used glycerol as a proxy for water in studies of the gas-liquid interactions relevant to atmospheric aerosol chemistry and published much work on interfacial proton exchange between halide acids in the gas phase and glycerol in the presence of alkali halide salts.[1,4,5,54-56]

In contrast, interfacial characteristics of halide aqueous solutions have been extensively studied. For example, Jungwirth and Tobias used MD simulations to study and predict ion surface propensity and solvation at the interface between air and aqueous halide solutions.[57,58] Later, Liu et al., using VSFG as well as IR and Raman spectroscopy,

investigated the ion distributions at the surface of aqueous halide solutions and revealed structural differences relative to the neat air/water interface.[59] Baldelli et al.,[60] Raymond et al.,[61] and Tian et al.[62] also used VSFG spectroscopy to probe the hydrogen bonding of aqueous halide solution surfaces. Additionally, Bian et al. also examined the perturbation of various halides on interfacial water organization by using surface second harmonic generation (SHG) spectroscopy.[63]

In this thesis, we present spectra of sodium halide glycerol solutions in the OH stretching vibrational region using VSFG, Raman, and IR spectroscopy. By comparing the glycerol spectra with spectra of aqueous solutions, differences and similarities associated with glycerol and with water, as well as their interactions with halide anions, are analyzed and discussed. In addition, surface tension measurements on the same solutions have been performed to assess the surface propensity of the given solutes. The research presented here was motivated by prior work conducted by Nathanson and coworkers.[4,54,55] Our findings reveal many similarities between aqueous and glycerol solutions with respect to ion surface propensity of halide salts and solvation.[9-11,21-23]

4.2. Experimental section

Materials. Sodium bromide (certified ACS granular, 99.5% purity) and sodium iodide (certified crystalline) were purchased from Fisher Scientific. For purification, all salts were heated at 500 ^{o}C for 10 h before dissolving in solvents. Glycerol (≥99% purity) was purchased from Sigma-Aldrich. Nanopure water (not purged of CO_2) with a pH of 5.5

and a resistivity of 18.0 MΩ·cm was obtained from a Barnstead Nanopure system (model D4741, Thermolyne Corporation) equipped with additional organic removing cartridges (D5026 Type I ORGANICfree Cartridge Kit; Pretreat Feed).

Preparation of Salty Solutions. Halide salt aqueous solutions were prepared by simply dissolving the purified salts in nanopure water. Halide salts were dissolved overnight in the same manner in glycerol assisted with a magnetic hotplate and a stirrer. For convenient comparison with Nathanson's studies,[4,5] 1 M and 2 M salt solutions were chosen for both water and glycerol. NaCl was not selected due to its relatively low solubility in glycerol at these concentrations. In addition, all solutions were conditioned at room temperature (23 ± 1 °C) over 24 h prior to any measurement.

VSFG Spectroscopy. VSFG spectroscopy measurements were performed using a broadband VSFG spectrometer setup that has been described in Chapter 3.

Raman Spectroscopy. The Raman experimental setup consisted of a 532 nm continuous wave laser (Millennia Vs, SpectraPhysics), a Raman probe (RPS532/12-15, InPhotonics), a monochromator (SR-303I-A, Andor Technology; 1200 g/mm grating), and a CCD (Newton EM, DU970N-BV, Andor Technology). Raman spectra were collected in the 0° backscattered direction using a fiber optic which was coupled to the entrance slit of the monochromator. Andor SOLIS software (version 4.15) was used for data collection and display. The output power of the 532 nm beam exiting the Raman probe was ~95 mW. Prior to data collection, the Raman system was calibrated with a USB Ne-Ar source (Princeton Instrument) and further fine-calibrated by taking the Raman spectrum of

naphthalene powder. Raman spectra were obtained using unpolarized light as the multimode fiber scrambles the polarization from the laser. All samples were prepared in 4 mL pyrex glass vials. All Raman spectra were obtained at room temperature.

FTIR Spectroscopy. An FTIR spectrometer (Spectrum 100 FTIR Spectrometer, Perkin Elmer) was employed in the attenuated total reflection Fourier transform infrared (ATR-FTIR) spectroscopy measurements using a 45° incident geometry and a ZnSe crystal mounted to the bench-top of the FTIR spectrometer. Although ATR-FTIR is usually used for interfacial measurements, it was employed here as a bulk interrogation technique due to the fact that the penetration depth using the ATR crystal is on the order of micrometers. In comparison to transmission IR, the ATR mode has also for advantage to avoid signal saturation in the OH stretching region. For each solution, a volume of about 1 mL was deposited on the crystal surface. Spectra were collected using Spectrum Software (version 6.3.4) with a spectral resolution of 4 cm^{-1} and 100 scans at room temperature.

Surface Tension Measurements. Surface tension was measured using a surface force device from a Langmuir trough system (Minitrough, KSV Instruments). A platinum Wilhelmy plate (measured perimeter of 39.4 mm) was cleaned with concentrated sulfuric acid and flamed using a Bunsen burner before measurements to ensure removal of adsorbed adventitious organic contamination.[64] Measurements were taken by pouring ~12 mL of salty solutions into a petri dish and dipping the plate into the liquid surface. Care was taken to place the plate in the center of the dish upon contact with the surface to avoid meniscus effects. The force exerted on the plate was read in KSV LayerBuilder software (version 2.0.1) and the surface tension was calculated using the Wilhelmy equation.[64]

4.3. Results and discussion

There have been relatively few studies investigating the air/glycerol interface by means of VSFG spectroscopy[49,50] and none so far reporting VSFG spectra of halide salt glycerol solutions. Here VSFG spectra of NaBr and NaI glycerol solution surfaces are determined in the OH stretching region to understand interfacial organization and solvation for this protic solvent. The OH group is highly sensitive to its environment,[30,31,34,65-68] in particular to solvation of halide anions at the air/glycerol interface and in the bulk phase.[30,37,60,61,69,70] To this end, the VSFG spectra of pure glycerol and water surfaces, essential in understanding interfacial organization of the solvated salt ions, are first shown, followed by bulk measurements using Raman and IR spectroscopy for comparison. Finally, surface tension data on salty glycerol solutions are presented to further discuss halides' surface prevalence.

4.3.1. Glycerol and Water. The VSFG spectra of the neat air/glycerol and air/water interfaces in the OH stretching region (3000-3800 cm^{-1}) are shown in Figure 4.1. Both VSFG spectra exhibit broad overlapping resonances extending from 3000 to 3550 cm^{-1} that are assigned to the hydrogen-bonded OH groups of glycerol and water at their respective air/liquid interfaces. The broad band for glycerol is somewhat asymmetric in character with stronger and weaker intensity in the lower (~3100-3300 cm^{-1}) and higher (~3300-3550 cm^{-1}) frequency regions, respectively. Possible contributions from the CH resonant tail cannot be ruled out. The water broad band has more obvious structure and reveals relatively equal intensities for the range from 3150 to 3450 cm^{-1}. Spectral assignments for the neat water VSFG spectrum have been discussed extensively and

remain somewhat controversial, especially for the lower frequency region.[68,71-75] It is believed that the broad band ranging from 3000 to ~3600 cm^{-1} reflects the collective OH stretching modes of hydrogen-bonded water molecules that display complex coordination and cooperativity within a few Å below the topmost water surface layer.[35,62]

Additionally, by comparing with the neat water VSFG spectrum, one can notice in the glycerol spectrum the absence of the sharp peak located at 3700 cm^{-1}. This is a key spectral feature in the neat water VSFG spectrum that has been assigned to dangling OH groups that protrude out into the vapor phase and comprise ~25% of the topmost surface water molecules.[76,77] The lack of a similar spectral feature in the glycerol spectrum indicates the absence of dangling OH groups, although this does not preclude other considerations such as a possible isotropic orientation or parallel (anisotropic) orientation of these groups in the surface plane. Both of these scenarios are difficult to rule out due to low signal-to-noise ratios of complementary VSFG polarization studies.[50] A molecular dynamics study of the glycerol surface revealed that it is more likely to find CH and CH_2 groups than the glycerol oxygens (OH groups) at the neat glycerol surface.[78] This is consistent with the small VSFG signal intensity found in the high frequency region of the VSFG spectrum. Moreover, based on findings from VSFG spectra of glycerol and other alcohols, Baldelli et al.[49,50] and Stanners et al. (for studies of methanol and ethanol)[79] also suggested that very few dangling OH bonds should be exposed at the neat glycerol surface.

Although the apparent spectral shape and bandwidth of the glycerol VSFG spectrum in the OH stretching region is obviously different from that of water, it still suggests that there are strong and weak hydrogen bonds as one moves from the low to the

high frequency region. The narrower band of glycerol relative to water is indicative of narrower distribution of hydrogen bonding strengths. Additionally, the overall intensity of the glycerol spectrum is slightly lower than that of water, suggesting a lower OH density relative to neat water, as is expected due to the replacement of water by glycerol. Yet, variation from interference effects inherent with VSFG spectroscopy,[30,31,33,80,81] oscillator strength, and reduced signal from increased scattering due to glycerol aggregation states should also be considered.[44,46,82] A similar intensity reduction was also observed in a previous study of water and ethanol using VSFG spectroscopy.[83]

4.3.2. Salty Glycerol and Water Solutions. To understand the effect of halide anion on glycerol interfacial solvation, VSFG spectra of two salty glycerol solutions (NaBr and NaI) at two different concentrations (1 and 2 M) were studied (Figure 4.2a), together with the spectrum of pure glycerol as reference. The VSFG spectra of the salty glycerol solutions have a similar asymmetric spectral shape as that of pure glycerol with a larger signal enhancement in the lower frequency region, but differ significantly in their overall signal intensity. Note that for the glycerol solutions, the 2 M NaBr is similar in intensity to the 1 M NaI, but in general, there is an increase in intensity with concentration given the same salt.

A comparison between the 1 M NaBr and NaI glycerol VSFG spectra shows a similar intensity increase in the low frequency region centered at 3250 cm^{-1} for both anions, while the higher frequency region above 3400 cm^{-1} experiences a slightly larger intensity increase in the case of I^- ions (Figure 4.2a). The enhancement in the higher frequency region thus appears to be strongly ion- and concentration-dependent. These intensity

observations suggest a correlation to halide anion size and polarizability where increasing size and polarizability give rise to increasing intensity. This is reminiscent of previously published results from aqueous halide surfaces.[59] The relatively large noise at 3600-3800 cm^{-1} in the VSFG spectra of glycerol solutions is due to the lower energy at the high frequency side of the IR laser pulses used in the experiments. Particularly, the noise associated with the 2 M NaI is higher than others, and likely arises from light scattering of the concentrated solution.

For comparison to the aqueous salt solutions, the VSFG spectra of the OH stretching region of 2 M aqueous NaBr and NaI in the OH stretching are shown in Figure 4.2b, with the neat water spectrum shown for reference. As with the salty glycerol spectra (Figure 4.2a), an enhancement of the intensity is also observed in these spectra, but solely in the higher frequency region. However, the 2 M NaI solution VSFG spectrum is enhanced more than the 2 M NaBr solution. This observation is consistent with previously published work.[59,61] The dangling OH intensity remains generally unchanged for aqueous NaBr and NaI.

The signal enhancement in VSFG spectra observed for both salty glycerol and aqueous solutions reveals that the OH stretching band is highly sensitive to the incorporation of the halide anions within their interfaces. These spectra also indicate that the enhancement varies with the halide anion identity and that increasing the concentration also increases the enhancement for each sodium halide measured, thus revealing similarities in solvation characteristics between glycerol and water. However, the halide salts increase the intensity in the lower frequency region of the salty glycerol spectra, but

a decrease is seen in the corresponding salty aqueous spectra. This might suggest that the halide salts reorganize differently the hydrogen bonding network of glycerol than for water. This is discussed further below. However, this assertion would clearly need further experimental and computational verifications beyond the scope of the current study; phase-sensitive VSFG (PS-VSFG) spectroscopy studies are underway in our laboratory to test this.

Yet, in order to further explore the origins of this VSFG signal enhancement, comparison of the VSFG spectral signature with that from bulk Raman and IR spectroscopic measurements is helpful. This comparison is justified by the fact that the (orientationally averaged) molecular hyperpolarizability (β_{ijk}), which is proportional to the VSFG intensity, is related to the product of Raman polarizability (α_{ij}) and IR dipole (μ_k) transition moment strength of interfacial molecules:[80]

$$\beta_{ijk} = \langle g|\alpha_{ij}|\nu\rangle\langle\nu|\mu_k|g\rangle \quad (1)$$

where ν and g are the excited and ground vibrational states, respectively. This gives rise to the VSFG selection rule according to which any vibrational mode of an interfacial species must be both Raman and IR active in order to be VSFG allowed. Therefore, Raman and IR spectroscopic evaluation of the salty glycerol solutions provide knowledge of the bulk solvation environment, and also provide a basis for comparison for the interfacial presence of the ions because of the theoretical relationship between Raman and IR with VSFG.

The Raman and Raman difference spectra of pure glycerol, and 1 M and 2 M sodium halide glycerol solutions were measured and are shown in Figure 4.3. The pure glycerol exhibits a broad OH stretching band consisting of two main peaks at ~3260 cm^{-1} and ~3460 cm^{-1}. Based on polarization Raman studies, Mendelovici et al. analyzed this broad band and decomposed it into two subpeaks at 3240 cm^{-1} and 3407 cm^{-1}, which were assigned to symmetric and antisymmetric OH stretches, respectively.[47] In contrast, Kojima[46] and Mudalige and Pemberton[84] fit the Raman spectrum in this region to three subpeaks centered respectively at 3230 cm^{-1}, 3340 cm^{-1} and 3440 cm^{-1}. The former two were assigned to the OH vibrations of oligomers with an aggregation number greater than two, while the latter one was associated to the modes of dimeric units.[46,84] Here, similarly to the assignment of water Raman spectra, a more general assignment of the OH stretching of glycerol is made where lower and higher spectral frequency regions are thought to be representative, respectively, of strongly and weakly hydrogen-bonded solvent networks.

With respect to the salty glycerol solutions shown in Figure 4.3a, an increase in Raman intensity is associated with anion identity (size and polarizability) and concentration, which is consistent with previously published Raman data of halide ions in methanol.[85] In addition, the Raman spectral changes induced by the solvated salts, namely an increase in intensity with halide type and concentration appear similar to those observed for the aqueous halide solution spectra,[59] as shown in Figure 4.3c. This similarity is also emphasized by the salty water difference spectra shown in Figure 4.3d. Finally, one can note the small blue and red shifts of the 3200 cm^{-1} and 3450 cm^{-1} peaks, respectively, for

the salty glycerol spectra, although difficult to discern due to the broad character of the glycerol higher frequency region and the intensity decrease of the lower frequency band.

Based on the comparison between salty glycerol and aqueous solutions Raman spectra, the significant increase at ~3450 cm^{-1} is highly suggestive of an increase in the OH Raman transition moment strength. Recall that the 3400 cm^{-1} region is correlated with an increase in anion size and polarizability,[59] for both solvents. For salty water solutions, this observation has been explored in the literature experimentally[59,86] and theoretically.[86] Thus, the Raman spectral differences of Figure 4.3 are attributed to differences between the solvation of halide anions in glycerol versus that of water, although both solvents are thought to prefer monodentate binding.[52,87] Using MD simulations and Raman spectroscopy of halide aqueous solutions, Smith et al. proposed that the electric field effects on the first solvation shell result in the most significant changes in Raman spectra due to dissolved salts.[86] Thus, one might conclude that both the similarities and the differences between the Raman spectra shown here of salty glycerol and aqueous solutions results from the character of the hydrogen bonding in the first solvation shells of glycerol and water solutions. Given that larger differences are observed in the aqueous solution Raman spectra when comparing Figure 4.3b and 4.3d, it is suggested that water molecules are slightly more perturbed by the addition of halide salts relative to glycerol in the bulk environment (see Figure 4.3d, 3200 cm^{-1} region). In other words, water is more easily reorganized by the ions, as might be expected due to the fact that glycerol-glycerol interactions involve additional van der Waals forces (as these become larger as the mass and size increase), and per molecule, glycerol has additional sites for hydrogen bonding. Yet, both solvents appear

to be impacted primarily in the higher frequency region, suggesting somewhat similar solvation properties. The enhanced intensity change in more concentrated salty glycerol solutions (as well as in water) can be readily understood due to the increased number of ions interacting with solvent molecules.

The IR spectra of salty glycerol and aqueous solutions as well as their IR difference spectra are shown in Figure 4.4. The spectra of glycerol and its salty solutions show a very broad band around 3300 cm^{-1} (Figure 4.4a). Less intensity enhancement is observed here relative to the Raman spectra although the bands are blue-shifted relative to pure glycerol and pure water (Figure 4.4a and 4.4c). From the IR difference spectra Figure 4.4b and 4.4d, the intensity changes at ~3200 cm^{-1} and ~3400 cm^{-1} are somewhat comparable in both glycerol and water, although slightly more for water in the low frequency region. The overall observed spectral differences in the Raman and IR spectra are generally attributed to their selection rules, polarizability change versus change in dipole moment during the vibration; however, just as observed in the Raman spectra for both solvents, water appears to be perturbed to a greater extent as evidenced by the slightly larger change in the IR spectra.

Comparison of the Raman and IR spectra to the VSFG data reveals that the VSFG spectral changes upon addition of the salts reflect in some ways the changes observed in the Raman and IR data. However, the VSFG intensity enhancement in the 3200 cm^{-1} region is not necessarily predicted from an analysis of the bulk spectroscopic data. In the interfacial region, the glycerol molecules may be oriented in an electric field as is now being suggested for other aqueous interfaces.[31,88-90] A study on $CaCl_2$ and NaCl aqueous

solutions combining conventional and phase-sensitive VSFG (PS-VSFG) spectroscopy study by Hua et al. might provide some insights.[89] PS-VSFG spectroscopy provides orientational information about the net OH transition moment from which ion distributions within the interfacial region can be inferred. In Hua et al.'s work,[89] an enhancement of the OH stretch region in the PS-VSFG Im $\chi^{(2)}$ spectra was observed in the spectra of $CaCl_2$ and NaCl aqueous solutions compared to pure water, and revealed that a greater alignment of interfacial water molecules was due to the presence of an interfacial electric field induced by the ion's spatial distribution. This interpretation is also supported by Tian et al.'s study on atmospherically relevant ions in salt solutions.[90] It can be argued here that halide salts possess similar effects at the air/glycerol interface, and that sodium and halide ion distributions create an electric field in the interfacial region that helps to align the glycerol OH groups (unpublished preliminary PS-VSFG data are suggestive of this). Since VSFG spectroscopy is interface specific and responsive to an environment lacking centrosymmetry such as an interface, the more ordered OH groups of interfacial glycerol molecules due to the electric field created by the separation of cations and anions could give rise to a higher intensity in VSFG spectra. This is supported indirectly by Cwiklik et al.[91] who investigated the surface of NaI solution of ethylene glycol using MD simulations. The density profiles showed that I^- ions mainly populated the interfacial region with their counter cations Na^+ located ~8 Å below them. This separation could create an interfacial region where the transition dipole moments of ethylene glycol OH groups, and similarly glycerol OH groups, become more aligned as well. As stated above, PS-VSFG data needs

to confirm this speculation, as the real part of the refractive index can obscure interpretation from conventional VSFG data.[89]

4.3.3. Surface Tension of Salty Glycerol and Aqueous Solutions. Considering that surface tension is a thermodynamic macroscopic indicator of the surface prevalence for a given solute, it could provide complementary information for the above-discussed molecular-level spectroscopic results regarding sodium halides. The surface tension measurements of NaBr and NaI glycerol and aqueous solutions relative to the pure solvents are shown in Figure 4.5. For the salty glycerol and aqueous solutions, an increase in the surface tension with increasing concentration is observed. However, the surface tension of salty glycerol solutions does not increase to the same extent as that from aqueous solutions. This is not necessarily surprising because glycerol is expected to be surface active. Halide surface accumulation followed by a depletion region in the interface is consistent with theoretical work by Jungwirth and Tobias.[57,58] The increase relative to pure water in the presence of sodium halides is obviously higher than that relative to pure glycerol. However, the trend that I^- ions produce a less significant surface tension increase compared to Br^- ions holds for both glycerol and water, suggesting that I^- ions segregates more than Br^- ions to the surface.[57,58,92]

4.3.4. PS-VSFG Spectra of Glycerol and Salty Glycerol Solutions. As mentioned earlier, PS-VSFG can provide information about the molecular orientation in the interfacial region. Preliminary PS-VSFG spectra (ssp-polarized) of glycerol and salty glycerol solutions are presented in Figure 4.6 and Figure 4.7. The PS-VSFG spectrum of water shows a negative band at 3200-3600 cm^{-1}, which indicates a structure of OH dipoles

pointing down to the liquid phase. The first PS-VSFG spectrum of water reported by Shen and coworkers showed a positive sign at lower region (<3200 cm^{-1}) and a negative sign at higher region (3200-3600 cm^{-1}), which was interpreted as upward OH bonds into the air and downward OH bonds into the water, respectively.[31] Although the spectrum here is consistent with Shen and coworkers' work, the interpretation of OH stretching region in PS-VSFG water spectrum is still controversial.[93,94] Surprisingly, the PS-VSFG spectrum of glycerol exhibits a positive sign at 3200-3600 cm^{-1}, opposite to what is observed for water. This difference suggests that the OH bonds in the interfacial glycerol molecules are mostly oriented in an opposite direction as in water, that is, pointing towards the air phase. Baldelli and Schnitzer proposed in their VSFG study of air/glycerol interface that the carbon chain of glycerol is perpendicular to the surface plane.[49] However, how the orientation of OH bonds in glycerol is related to that of carbon chain is still unclear, and the detail about the interfacial glycerol structure requires support from more PS-VSFG experiment and computational studies.

Upon addition of sodium halide salts to glycerol, the PS-VSFG spectra of salty glycerol solutions are significantly changed, as shown in Figure 4.7. The spectrum of 2 M NaI glycerol solution remains positive at 3200-3600 cm^{-1} as neat glycerol. However, the sign is changed to negative in 2 M NaBr glycerol solution, which seems to have a more pronounced impact on the OH bonds in glycerol than the NaI glycerol solution. This is different from the spectra obtained in conventional VSFG. Shen and coworkers have reported the PS-VSFG spectra of NaCl and NaI aqueous solutions, which show a more significant increase relative to water in the presence of NaI over NaCl.[90] The difference

between the halide glycerol and aqueous solutions may indicate that the halide salts have different effects on the OH bonds in corresponding liquids. Although the interpretation of change of PS-VSFG spectra in halide glycerol solutions relative to water is still unknown, NaBr and NaI clearly affect differently on the OH bonds in interfacial glycerol molecules.

4.4. Conclusions

Here, bromide and iodide anions are shown to exist at the air/glycerol interface and to perturb the glycerol hydrogen bonding network. The more polarizable halide I^- has a larger impact on the VSFG spectrum in the OH stretch region relative to Br^-, suggesting a larger surface propensity of I^- than Br^- in the air/glycerol interfacial region. However, the difference observed at ~3200 cm^{-1} between the air/glycerol and the air/water VSFG spectra, indicates a different distribution of hydrogen bonding strengths in the interfacial region. Additionally, surface tension measurements suggest a similar trend in surface excess of halide anions for the air/glycerol and air/water interfaces. Moreover, the VSFG results reveal that glycerol and water share similar trends in terms of hydrogen bonding disruption, but their impact on water organization in the interfacial region in the presence of halide anions is slightly different. Additional experiments (phase sensitive VSFG and possibly high pressure X-ray photoelectron spectroscopy) in addition to theoretical work would be advantageous to further investigate the relative propensity of halide anions at the air/glycerol interface.

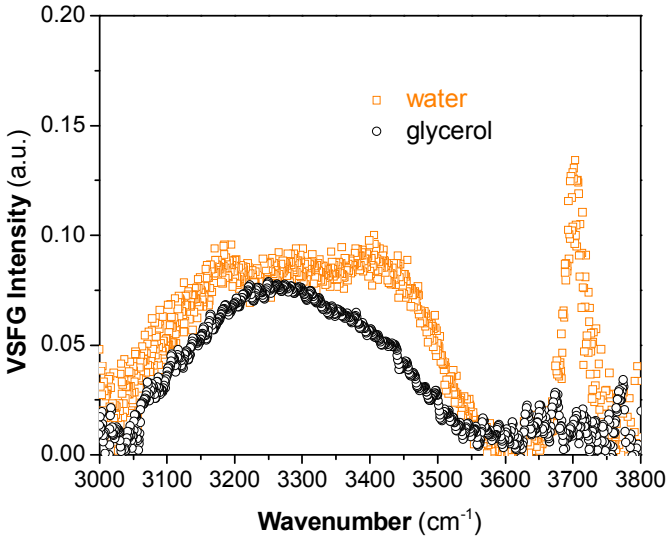

Figure 4.1. VSFG spectra of the neat air/water and air/glycerol interfaces in the OH stretching region (3000-3800 cm^{-1}). Glycerol spectrum was smoothed using a 15 data points Savitzky-Golay filtering.

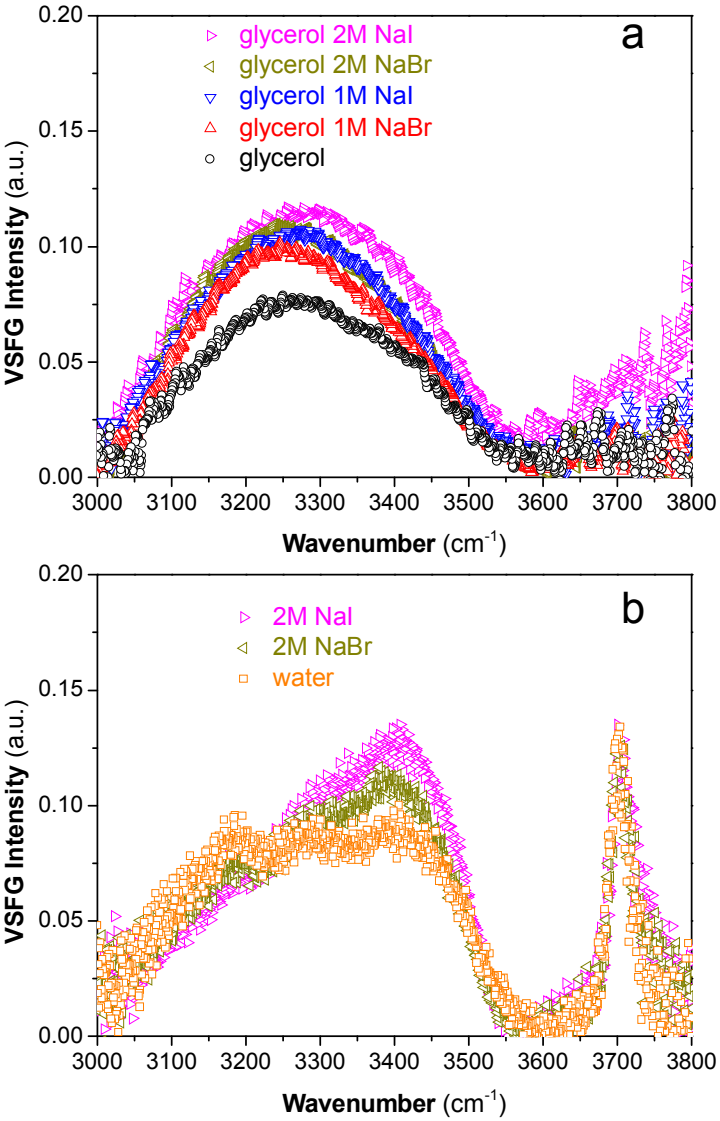

Figure 4.2. (a) VSFG spectra of sodium halide glycerol solutions in the OH stretching region (smoothed using a 15 data points Savitzky-Golay filtering). (b) VSFG spectra of sodium halide aqueous solutions in the OH stretching region. The VSFG spectra of neat glycerol and water are also shown as reference.

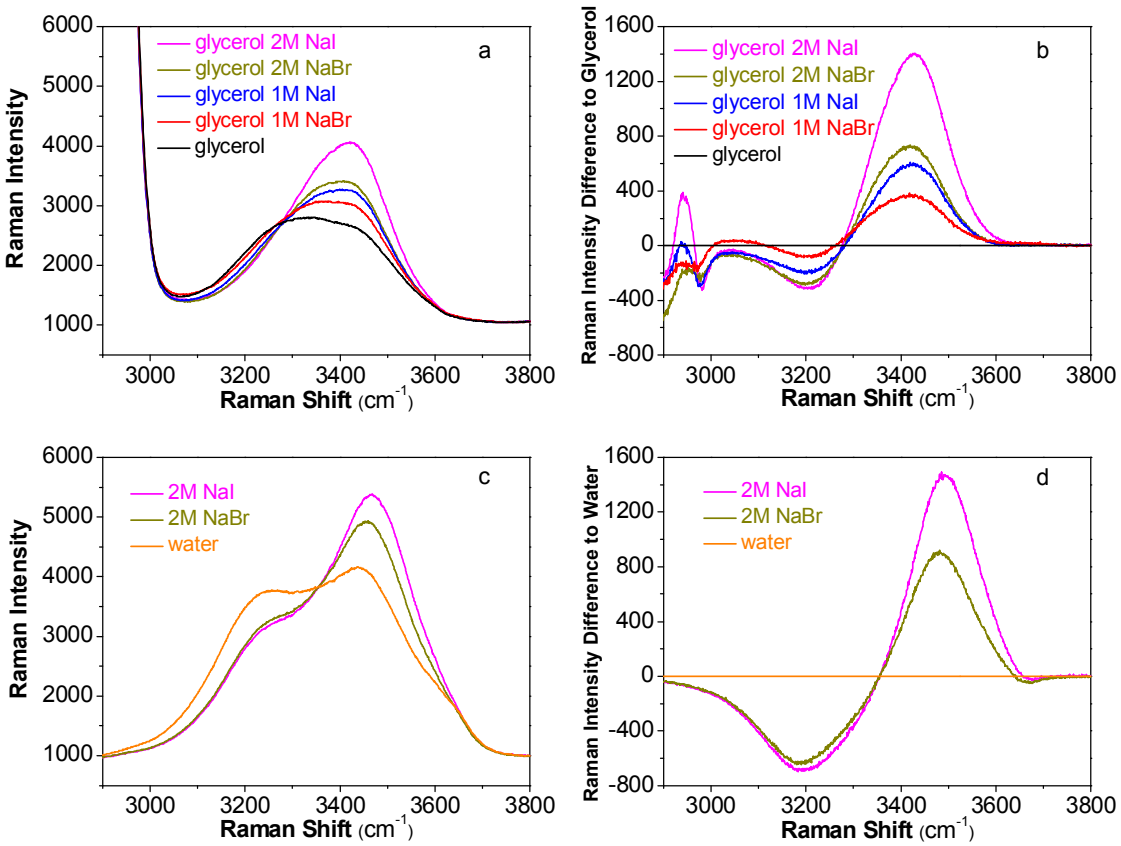

Figure 4.3. (a) Raman spectra of sodium halide glycerol solutions. (b) Raman difference spectra of sodium halide glycerol solutions relative to pure glycerol. (c) Raman spectra of sodium halide aqueous solutions. (d) Raman difference spectra of sodium halide aqueous solutions relative to pure water.

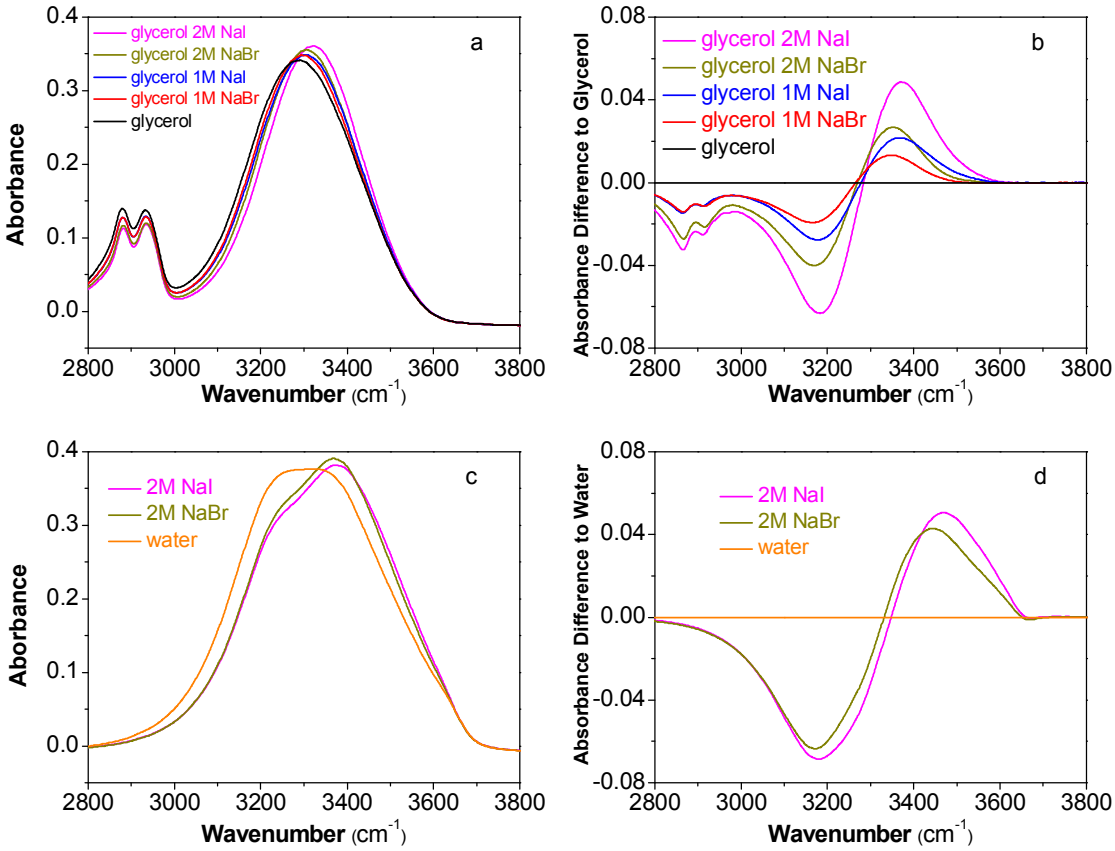

Figure 4.4. (a) FTIR spectra of sodium halide glycerol solutions. (b) FTIR difference spectra of sodium halide glycerol solutions relative to pure glycerol. (c) FTIR spectra of sodium halide aqueous solutions. (d) FTIR difference spectra of sodium halide aqueous solutions relative to pure water.

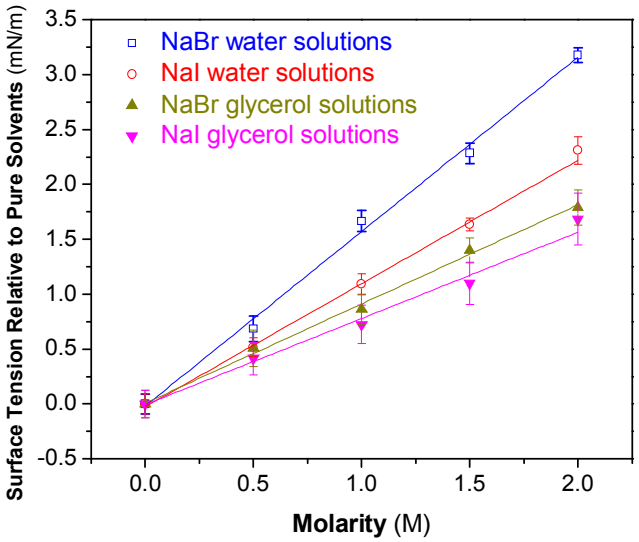

Figure 4.5. Surface tensions of sodium halide glycerol and aqueous solutions relative to their respective pure solvents.

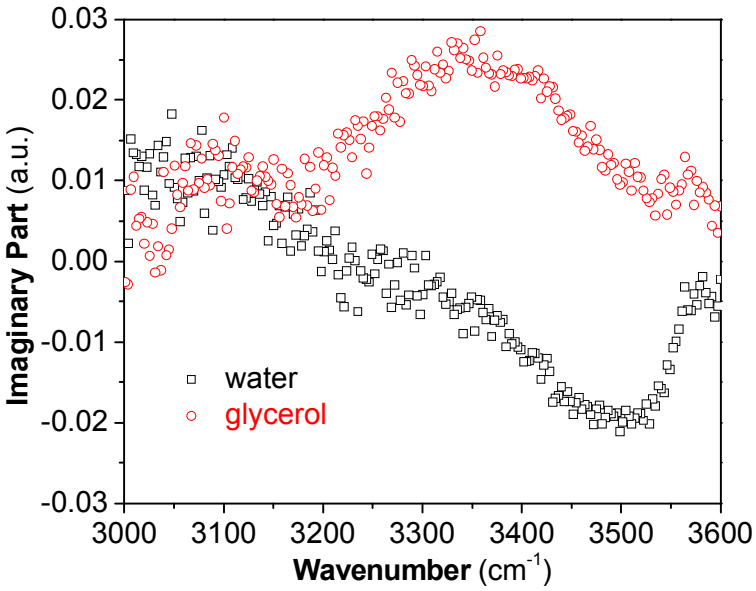

Figure 4.6. PS-VSFG spectra of water and glycerol.

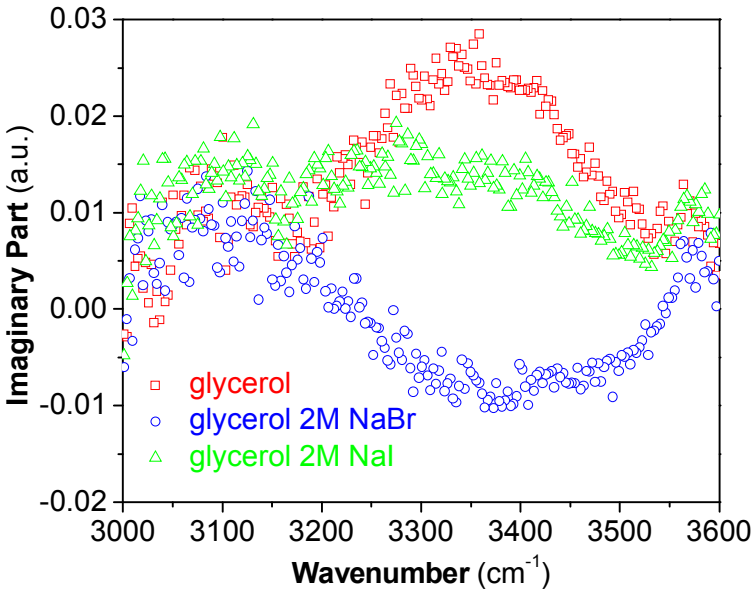

Figure 4.7. PS-VSFG spectra of glycerol and salty glycerol solutions.

Chapter 5: Influence of Salt Purity on Na^+ and Palmitic Acid Interactions

5.1. Introduction

Cation-specific effects in aqueous solutions are essential to many chemical, biochemical, and atmospheric processes.[9-16] Particularly, Na^+ and K^+, as the two most abundant alkali cations in intra- and extracellular fluids, play a critical role in cell signaling.[17-19] While both are alkali cations, they exhibit notable chemical differences, e.g. the intra- and extracellular Na^+/K^+ ratios as regulated by ion pumps in cell membranes.[95-98] Jungwirth and coworkers have shown that the preferred interactions of Na^+ and K^+ with proteins can be attributed to the stronger affinity of Na^+ for the carboxylate groups (COO^-) in protein side chains.[22,29] Jagoda-Cwiklik et al. extended the computational work to other anionic groups in discriminating Na^+ and K^+ affinities in biological environments.[23] This was in agreement with the "law of matching water affinities" for which anions and cations with similar size and valence preferentially form stable ion pairs.[99] Other computational analyses of the cation-carboxylate interactions have shown stronger preference of Na^+ to COO^- relative to K^+.[20,25,28,100,101]

In addition to these theoretical studies, experimental work has been undertaken to elucidate the cation binding to the carboxylate group. For instance, Simon-Kutscher et al. and Le Calvez et al. studied the ionic binding of stearic acid with various aqueous divalent

cations using infrared reflection-absorption spectroscopy (IRRAS),[24,26] while Uejio et al. and Aziz et al. examined the cation-specific interactions with COO^- in aqueous solutions using X-ray absorption spectroscopy.[20,28] More recently, Murdachaew et al. investigated the alkali cation interactions with dicarboxylate dianions in the gas phase by photoelectron spectroscopy.[25] Cremer and coworkers utilized surface-specific vibrational sum frequency generation (VSFG) spectroscopy and studied the interactions between cations and carboxylate groups at air/aqueous interfaces.[13,21] Most of the results obtained with Na^+ and K^+ ions have suggested that Na^+ has a stronger binding affinity to COO^- relative to K^+.[13,20,25,28] Another VSFG spectroscopy study, however, by Tang and Allen, pointed out a greater affinity of K^+ than Na^+ for the COO^- group of palmitic acid.[16] This controversial finding initiated further experiments probing the effect of high-valence contamination and their impact on such studies.[102] Aside from instrumental and methodological factors, the purity of the salts utilized in the experimental work was evaluated for their spectroscopic impact. As shown in Table 1, salts with different purities and pretreatment have been used among research groups. Note that there is typically a 1-2% contamination level in the ACS grade salts, part of which are polyvalent cations such as Mg^{2+}, Ca^{2+}, Fe^{3+}, Pb^{2+}, and Ba^{2+}. The presence of such polyvalent cations, even in trace amounts, could significantly alter the binding affinities of monovalent cations and perturb the interfacial water organization through binding to the carboxylate group.[21]

In fact, salt purity in the aforementioned and other relevant studies can be critical and may have a significant impact on the experimental results. Very recently, Hua et al. reported on the effects of salt purity on the interfacial water organization of various aqueous

salt solutions (in the absence of surfactant/lipid monolayer) using conventional and phase-sensitive VSFG spectroscopy.[102] Their results showed no appreciable difference in the OH stretching region of spectra obtained from those salt solutions prepared from filtered ultrapure (UP) grade and ACS grade salts, thus indicating the negligible impact introduced by the presence of trace amount polyvalent cations. Incidentally, much less work has been done to address the impact of the trace amount of polyvalent cations at air/surfactant interfaces.[21]

In this work, we clarify the impact of salt purity on the study of binding between one alkali cation (Na^+) and the carboxylate group of fatty acids by means of VSFG spectroscopy on palmitic acid (PA) monolayers at air/aqueous interfaces. Our results reveal significantly different binding affinity of Na^+ cations with the headgroup of PA by using filtered UP versus ACS grade salt solutions as subphase. During the spectral monitoring, a small intensity decrease of the COO^- stretching peak is observed for the UP salt solution whereas a pronounced intensity increase is seen for the ACS salt solution. For the whole OH stretching region, the intensity remains low and constant for the UP salt solutions but undergoes a gradual decrease over time for ACS grade salt solutions. The different spectral behavior is likely due to the stronger affinity of polyvalent metal ions present in ACS grade salt.

5.2. Experimental Details

Materials. PA (≥99%) and acyl chain deuterated d_{31}-PA (98%) were purchased from Sigma-Aldrich and Cambridge Isotopes, respectively. ACS grade (≥99%) and UP grade (trace metals basis, 99.999%) NaCl salts were purchased from Fisher Scientific and Acros Organics, respectively. Nanopure water (not purged of CO_2) with a resistivity of 18.2-18.3 MΩ·cm and a measured pH of 5.6 was obtained from a Barnstead Nanopure system (model D4741, Thermolyne Corporation) equipped with additional organic removing cartridges (D5026 Type I ORGANICfree Cartridge Kit; Pretreat Feed). All containers and glassware were carefully cleaned using concentrated sulfuric acid with addition of a strong oxidizer, ammonium peroxydisulfate, and then thoroughly rinsed with nanopure water.

Preparation of Lipid and Aqueous Salt Solutions. The PA and deuterated PA solutions were prepared in a 1.5 mM concentration range by dissolution in spectroscopic grade chloroform (Sigma-Aldrich). Both UP and ACS grade NaCl salts were baked at ~600 °C for 10 h in a muffle furnace (Isotemp model 550-14, Fisher Scientific). Stock salt solutions were prepared by dissolving UP and ACS grade salts in nanopure water and then filtering twice using carbon-activated filters (Whatman Carbon Cap 75, Fisher Scientific) to remove organic impurities. Their concentrations were then standardized by Mohr titration.[103] Both solutions were proven to be free of organic impurities in the CH stretching region from 2800 to 3000 cm^{-1} (Figure 5.S1) and conditioned at room temperature (23±1 °C) over 24 h before use.

Equilibrium Spreading of PA Monolayers. PA monolayers were overspread (~10 μL) on water and salt solutions in Petri dishes (5 cm diameter). The PA monolayers on

water and salt solutions reached a mean molecular area of ~21 $Å^2$/molecule, which corresponds to a 2D ordered (tilted liquid-condensed) phase. Following spreading, 10 min was allowed for solvent evaporation, after which VSFG spectra were collected for ~1 h. The acquisition time for each spectrum was 5 min.

Vibrational Sum Frequency Generation Spectroscopy. The VSFG spectra were obtained from a broad band VSFG spectroscopy setup which has been described in Chapter 3.

5.3. Results and Discussion

In the following discussion, VSFG spectra of PA monolayers in the COO^- and OH stretching regions are presented. The COO^- peak directly reveals the binding of the Na^+ cation to the headgroup of PA, while the OH stretching band relates to the interfacial water structure which is affected by the surfactant,[21,33,34,67,104,105] thus providing a complementary view of the binding event. Tang and Allen reported the VSFG spectra of PA on non-UP (e.g. ACS grade) salt solutions ~10-15 min after spreading and found a stronger affinity of K^+ for the carboxylate group over Na^+.[16] It is also known that the intensity of the spectra may change with time due to monolayer relaxation[27] that can affect the comparison of the binding affinity of cations to carboxylate groups. Therefore a time study was performed to see how the spectra change for aqueous solutions made from UP and ACS grade salts.

Direct Evidence of Na^+ Interactions with Carboxylate Group from the COO^- Stretching Region. Figure 5.1 shows the VSFG spectra in the COO^- stretching region of

a d_{31}-PA monolayer on 0.6 M NaCl solution ~1 h after spreading. Two peaks at ~1405 cm^{-1} and ~1470 cm^{-1} are observed for both UP grade and ACS grade salts. The d_{31}-PA was chosen here to avoid the interference from CH_2 bending modes (~1465 cm^{-1}). The contribution to the signal in this region is assigned to the different species of the COO^- groups. Note that the p*K*a value of the carboxylic acid group is ~4.85 in the bulk, but it increases to ~8.7 for long-chain fatty acids at the air/water interface.[27,106,107] Given a neat water subphase with pH 5.6, then according to the calculation reported by Shen and coworkers ~99.9% of the PA headgroups are mostly protonated prior to binding,[108] which is supported by the negligible SFG COO^- signal observed on neat water (Figure 5.1a). The presence of COO^- stretching signal observed in Figure 5.1b and 5.1c can be attributed to the deprotonation caused by the cations in the subphase,[16] which will be discussed below. The peak at 1405 cm^{-1} is assigned to hydrated species of COO^-,[16,27,108] whereas the one at 1470 cm^{-1} is indicative of ionic complexes of COO^- groups with cations.[16,27] This ionic complex has been previously identified by IRRAS.[24,26,109] The intensity of the high-frequency peak at ~1470 cm^{-1} is much higher than that of the low-frequency peak at ~1405 cm^{-1}, suggesting that most COO^- groups form complexes with the cations in the subphase. In the following discussion, the emphasis will be put on the 1470 cm^{-1} peak as it is directly related to the binding event between COO^- and Na^+.

Figure 5.1b depicts the VSFG spectra of PA monolayers on the solution prepared with the UP grade NaCl salt. After spreading, the 1470 cm^{-1} peak displays a gradual but small decrease in intensity (up to ~20%) and becomes relatively constant after about 1 h. Since the VSFG signal is responsive to ordered structures at interfaces,[80,81] the intensity

decrease here can be attributed to the monolayer relaxation that the PA molecules undergo; PA becomes more disordered as no counteracting surface pressure is applied. Sakai and Umemura also observed surface pressure relaxation in Langmuir monolayers of zinc stearate by infrared external reflection spectroscopy, which was linked to a change in the orientation angle of the hydrocarbon chain relative to the surface normal.[110] In addition, Ma and Allen's VSFG study on phospholipid monolayers on water showed a significantly lower intensity of the symmetric phosphate (POO^-) group at lower surface pressure (~12 mN/m),[111] which is similar to the COO^- intensity decrease observed here.

In the case of ACS grade NaCl salt, as seen in Figure 5.1c, the general features of the spectra remain nearly identical to those found in Figure 5.1b. The 1470 cm^{-1} peak in the initial spectra taken ~10 min after spreading is much lower in intensity than that of UP grade salt (compare black-line spectra in Figure 5.1b and 5.1c). Despite the different peak intensity ratio, the presence of two peaks at 1405 cm^{-1} and 1470 cm^{-1} in Figure 5.1c agrees with Tang and Allen's spectra (after ~10 min spreading).[16] However, unlike the intensity decrease of the 1470 cm^{-1} peak observed in the spectra from the UP grade NaCl solution, there is a remarkable intensity increase for the ACS grade NaCl solution, indicating that more cation-COO^- surface complexes are present and, thus, stronger cation binding to COO^-.[16,27] The intensity at ~1 h after spreading becomes constant and almost 6 times higher as the initial intensity although varying to some extent on different days (4 to 6 times higher; see Figure 5.S2). This trend is significantly different from that observed in the UP grade NaCl solution spectra. Since both ACS and UP grade NaCl salts were pretreated following the same procedure, and the experiments were performed under the same conditions, the

difference in intensity change can be primarily attributed to the purity of the salts, that is, the presence of small amounts of di- and trivalent cations which have stronger binding affinities with the headgroup of PA.[13,21,24,26,27] In particular, as shown in Table 1, the ACS grade NaCl contains more trace metals (>40 ppm) than UP grade NaCl (<10 ppm). It is expected that the small (<1%) but non-negligible amount of the polyvalent cations in the ACS grade salt bind to the COO^- groups due to their stronger binding affinity relative to Na^+,[13,24] which largely accounts for the dramatic intensity increase of the 1470 cm^{-1} peak with elapsed time.

Indirect Evidence of Na^+ Interactions with Carboxylate Group from the OH Stretching Region. The organization of water molecules in the OH stretching region is highly sensitive to its environment.[30,31,35,68,112,113] For instance, the influence of trace amount of organics on the interfacial water structure has been extensively studied.[21,33,34,67,104,105] Since all the salts used here are free of organics after pretreatment, the spectral change observed here can only be attributed to the cation-carboxylate binding.

Figure 5.2a presents the VSFG spectrum in the OH stretching region of a PA monolayer on neat water. There are four bands located at ~2940 cm^{-1}, ~3200 cm^{-1}, ~3450 cm^{-1}, and ~3600 cm^{-1}. The 2940 cm^{-1} peak is assigned to the Fermi resonance of the CH_3 symmetric stretch with the overtone of the bending mode.[16,108] The broad band from 3200 cm^{-1} to 3450 cm^{-1} is a signature of collective OH stretching modes of hydrogen-bonded water molecules that display complex coordination and cooperativity in the interfacial region.[35,114,115] The 3600 cm^{-1} peak results from weakly hydrogen-bonded OH groups of both fatty acid and water. These features are consistent with the VSFG spectra reported by

Miranda et al.[108] and Tang and Allen.[16,67] Although as mentioned earlier, most of PA molecules are intact at the water surface, a small amount of deprotonated carboxylic groups still exists, and, in turn, the presence of an electric field induced by this deprotonation can change the interfacial water structure,[67] as shown by the higher intensity relative to neat water in Figure 5.2a. Note that the spectra in Figure 5.2a are slightly different from previously reported spectra, especially from ~3600 to 3700 cm^{-1}.[16] This was probably caused by the lower energy on the high frequency side of our previous incident IR profile that is not easily normalized out.

In the presence of NaCl in the subphase, the VSFG spectra of the PA monolayers have significantly changed (Figure 5.2b and 5.2c). The intensity of OH stretching bands on UP grade NaCl solution (Figure 5.2b) changes dramatically relative to PA on neat water. Recalling that VSFG is responsive to ordered structures in an environment lacking inversion symmetry,[80,81] the lower intensity in the high frequency region in Figure 5.2b relative to Figure 5.2a indicates charge screening and that the hydrogen bonding between water molecules under the PA monolayer may be more disordered. In other words, the interaction of COO^- and Na^+ gives rise to a less charged interface that weakly aligns the water molecules. This explanation for the spectral intensity attenuation relative to PA on neat water is in accordance with previous VSFG studies of surfactant monolayers on salt solutions.[21,67,105,116] In addition, the intensity remains constant even 30 min after spreading the PA monolayer on the UP grade NaCl solution, suggesting that a stable monolayer is formed. It could serve as evidence that the trace amounts of polyvalent metal ions in the

UP grade NaCl salt did not result in a significant perturbation of the interfacial water organization.

In contrast, the VSFG spectra lineshape of a PA monolayer on ACS grade NaCl solution resemble that of PA on neat water (compare Figure 5.2a and 5.2c). The three broad bands in the region from 3000 to 3800 cm^{-1} are easily discernible and the peak assignment is similar to that on the neat water subphase, although the peak intensity decreases, especially at ~3200 cm^{-1}. The spectral intensity decrease provides evidence of cations binding to COO^-, as the water molecules become less aligned by the weaker interfacial electric field and the headgroup becomes less ordered with respect to orientation.[21,34,67,116] Despite the overall lower intensity relative to PA on neat water, the spectral intensity on ACS grade subphase is much higher at 3500 cm^{-1} than for PA on UP grade NaCl solution. As shown in Table 1, the concentrations of polyvalent cations in UP grade and ACS grade NaCl salts are 10 ppm and 40 ppm, respectively. Gurau et al. has reported the marked effect of trace amounts of divalent cations (1 and 10 μM) on a fatty acid monolayer in the OH stretching region relative to neat water.[21] It is expected that the impurity level of polyvalent cations between the UP and ACS grade salts in our experiment is sufficient and leads to the significant difference observed between Figure 5.2b and 5.2c.

The most significant difference between the UP and ACS grade salt solutions is the intensity changes with elapsed time. Unlike the VSFG spectra given in Figure 5.2b, those in Figure 5.2c decreased in intensity and then became unchanged after about 1 h. As more polyvalent metal cations present in the ACS grade salt, which have stronger binding affinity, bind to COO^- groups, hydrogen bonding structure changes. Accordingly, the ionic

complex between cation and COO^- becomes predominant and leads to an increasing peak at ~1470 cm^{-1} as shown in Figure 5.1c. The two complementary views of the binding mechanism revealed by the spectra from the COO^- and OH stretching region are consistent with each other.

Based on the spectral changes of PA monolayers on UP and ACS grade NaCl solutions in both the COO^- and OH stretching regions, the purity of alkali salts is found to have a great impact on the resulting spectra of fatty acids spread on their solutions (even after pretreatment). This may further cause difficulty in determining the relative binding affinity of cations, for example Na^+ vs. K^+. Therefore, UP alkali salts are highly recommended for studies of cation-carboxylate binding. Note that the impact of organic contaminants with the UP grade salt on the cation-carboxylate binding has not yet been studied.[13,14] Furthermore, to gain a better understanding of the cation-surfactant interaction, a complete study of other salts and surfactants (e.g. phospholipids) as well as of pretreatment effects is needed.

5.4. Conclusions

PA monolayers at the air/NaCl solution interface were monitored over time by VSFG spectroscopy in the COO^- and OH stretching regions after spreading on the pretreated solutions prepared from UP and ACS grade NaCl salts. Significant differences were observed between the UP and ACS grade salt solutions spectra. In the COO^- stretching region, the 1470 cm^{-1} peak, which is a signature of the ionic complex formed

between the COO^- group and cations, undergoes a small intensity decrease for the UP salt solution, whereas for the ACS salt subphase, a drastic intensity increase is observed. In the OH stretching region, the intensity of the broad band from 3000 to 3800 cm^{-1} remains unchanged for the UP salt solution but gradually decreases for the ACS one.

The information conveyed by the VSFG spectra of PA monolayers in the COO^- and OH stretching regions are consistent with each other. Both results demonstrate the impact of trace metal contaminants on the cation-carboxylate binding, and these impurities largely affect the spectra of PA in both spectral regions. The changes in the spectra for UP salt solution are related to monolayer relaxation, but for ACS salt subphase, the changes are likely due to the trace metal impurities that strengthen the cation-carboxylate binding. The grade of alkali salts therefore proves to be critical in exploring the cation-carboxylate binding and comparing relative binding affinity of different cations. The use of UP grade salt is strongly recommended especially in the studies related to alkali-carboxylate interactions. However, whether the salt purity effect applies to the interactions between other monovalent cations and negatively charged moieties such as the phosphate group in phospholipids is still unknown. More generally, special care should be taken in the selection of chemicals when investigating air/aqueous surfactant interfaces with surface-sensitive techniques. Finally, to further clarified the cation-surfactant interactions, more systematic work is needed.

Table 1. Salts with different purities and pretreatment used among research groups in studies of alkali cation-carboxylate interactions.

Salt/Carboxylate Source	Supplier	Grade and Purity	Salt Baking	Solution Filtration	Ref.
NaCl, KCl/Polypeptide	Sigma-Aldrich	NaCl: 99.999%, KCl: 99.999%	No	No	13
NaCl, KCl/Palmitic acid	Fisher Scientific	NaCl: certified ACS, 99% KCl: EP/BP/USP/FCC, 99%	No	Yes	16
NaCl, KCl/Protein	Lachema	p. a. grade	Not specified	Not specified	29
NaCl, KCl/Amino acid	Sigma-Aldrich	Highest purity commercially available	No	No	20
NaOH, KOH/Dicarboxylate acid	N/A	N/A	Not specified	Not specified	25
HCOONa, HCOOK, CH_3COONa, CH_3COOK	Sigma-Aldrich	98% or higher	No	No	28
NaCl/Palmitic acid (UP grade)	Acros Organics	Trace metals basis, 99.999% Polyvalent cations: <10 ppm	Yes	Yes	This work
NaCl/Palmitic acid (ACS grade)	Fisher Scientific	Certified ACS, 99% Polyvalent cations: ~40 ppm	Yes	Yes	This work

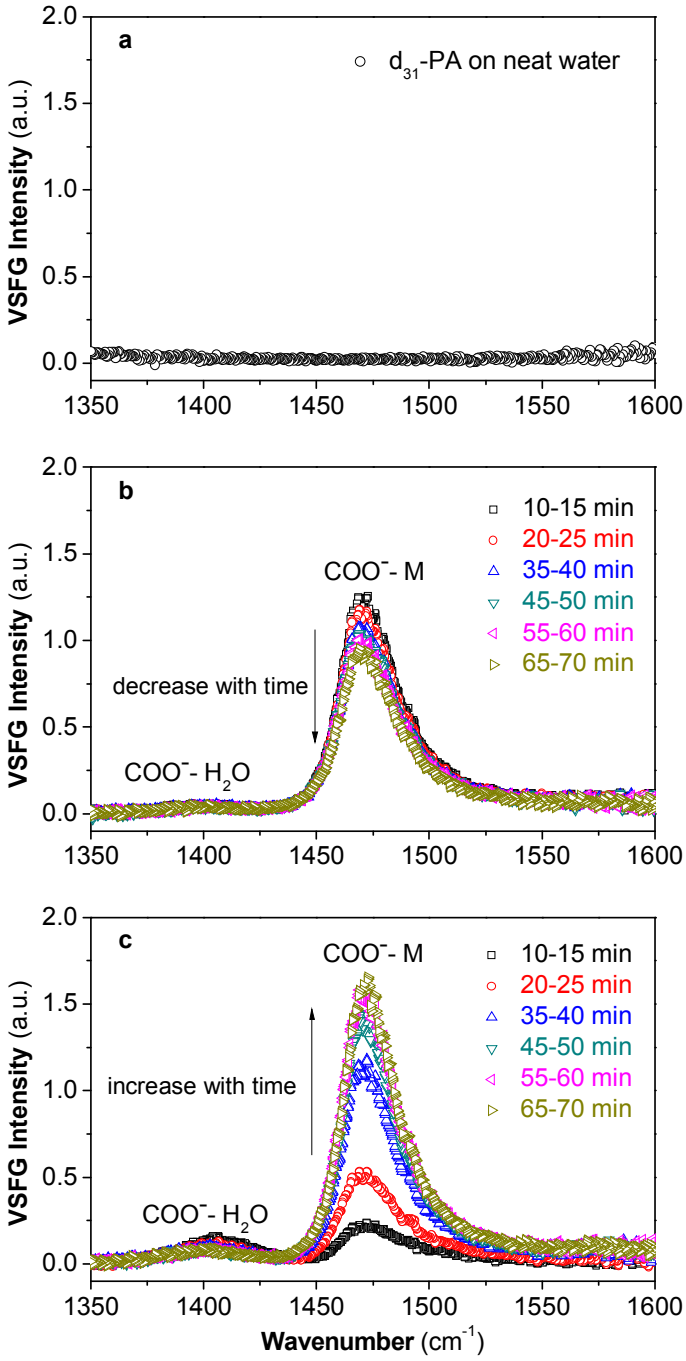

Figure 5.1. VSFG spectra of d_{31}-PA on 0.6 M NaCl solutions in the COO^- stretching region (1350-1600 cm^{-1}) ~1 h after spreading. (a) neat water. (b) UP grade 0.6 M NaCl solution. (c) ACS grade 0.6 M NaCl solution.

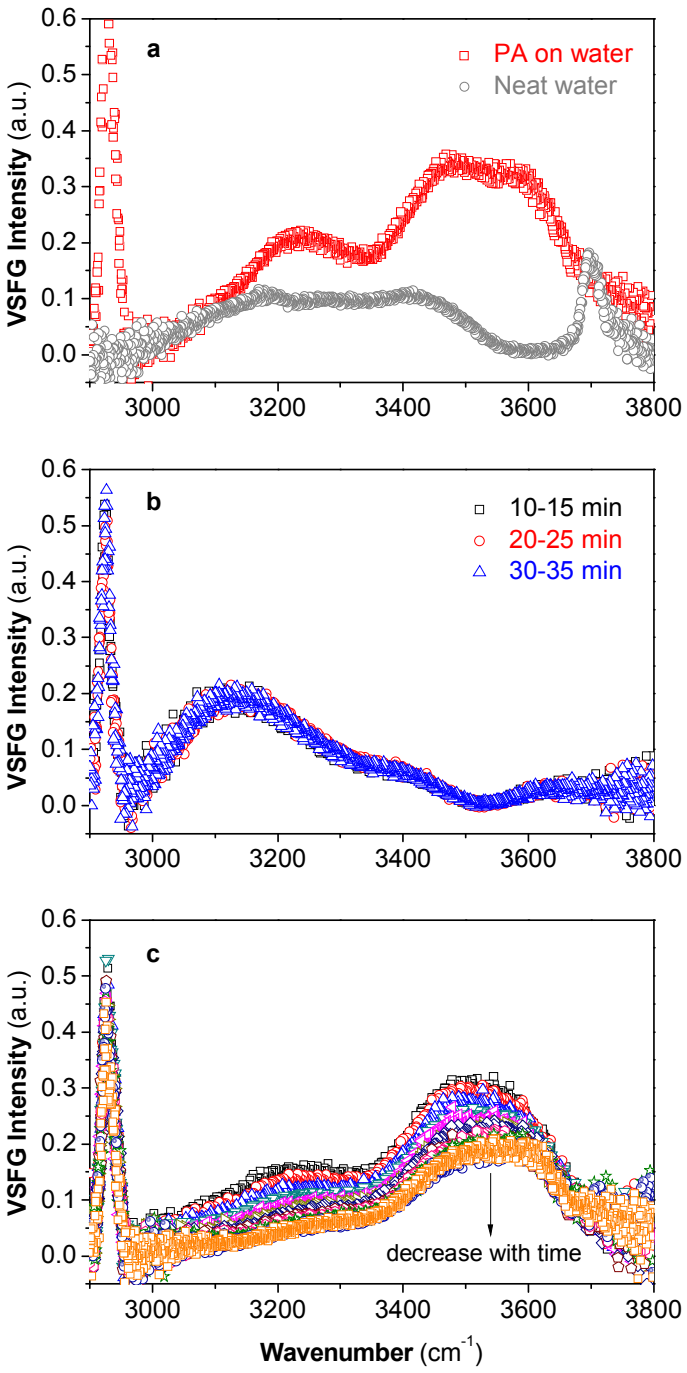

Figure 5.2. VSFG spectra of PA on pure water and 0.6 M NaCl solutions in the OH stretching region (3000-3800 cm^{-1}) ~1 h after spreading. (a) PA on water and neat water (b) UP grade 0.6 M NaCl solution. (c) ACS grade 0.6 M NaCl solution. Spectra were taken every 7 min on average ~10 min after spreading.

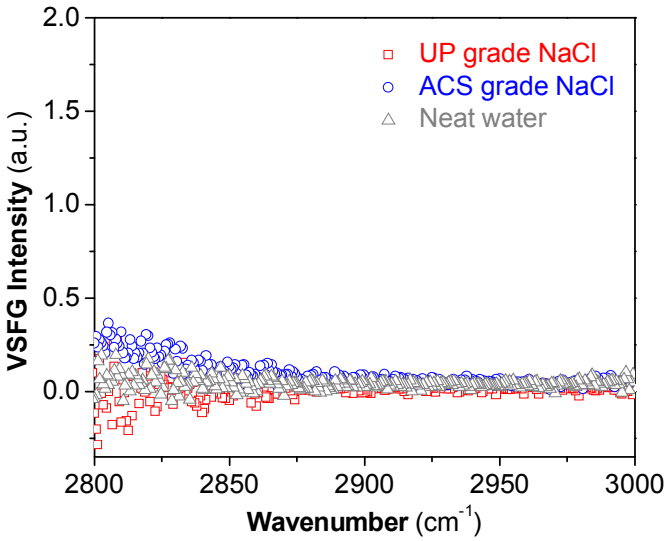

Figure 5.S1. VSFG spectra in the CH stretching region (2800–3000 cm^{-1}) of neat water and NaCl stock salt solutions studied after filtering 2 times.

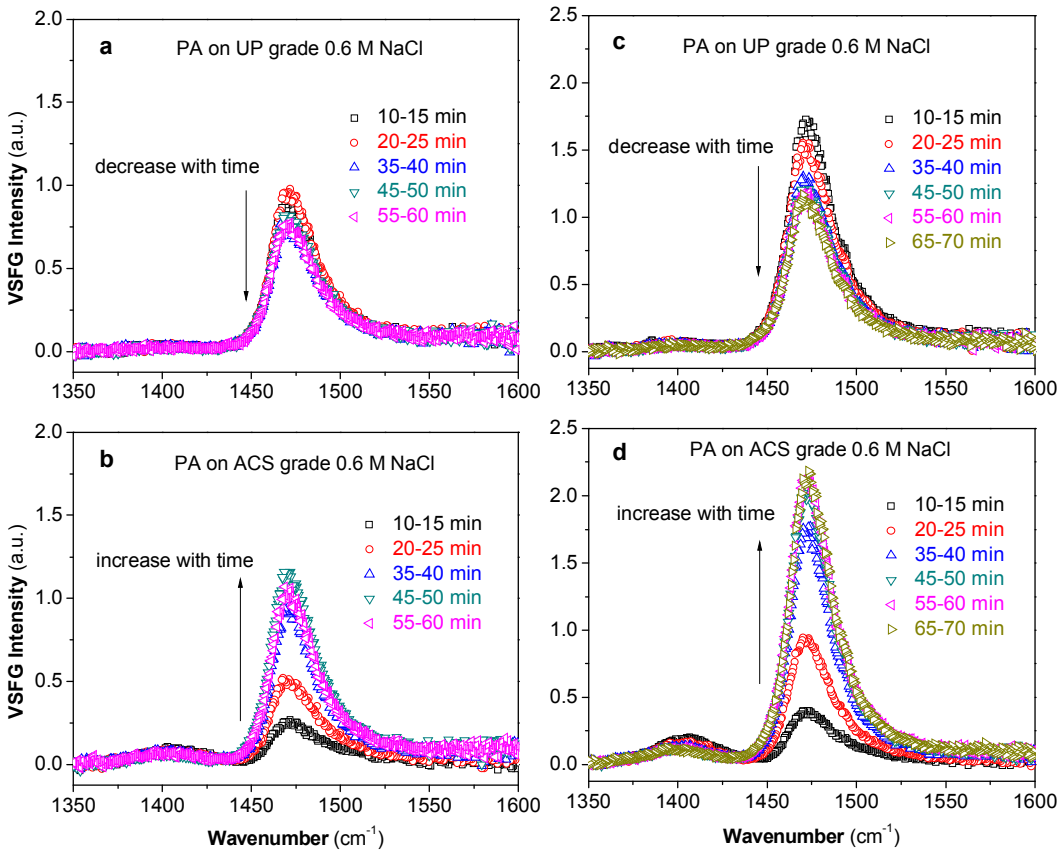

Figure 5.S2. VSFG spectra of d_{31}-PA on 0.6 M NaCl solutions in COO^- stretching region (1350–1600 cm^{-1}) ~1 h after spreading obtained on different days. (a) and (b) were from the day 2, (c) and (d) were from day 3. (a, c) UP grade 0.6 M NaCl solution. (b, d) ACS grade 0.6 M NaCl solution.

List of References

(1) Nathanson, G. M.; Davidovits, P.; Worsnop, D. R.; Kolb, C. E. *J. Phys. Chem.* **1996**, *100*, 13007.

(2) Saecker, M. E.; Nathanson, G. M. *J. Chem. Phys.* **1993**, *99*, 7056.

(3) Benjamin, I.; Wilson, M. A.; Pohorille, A.; Nathanson, G. M. *Chem. Phys. Lett.* **1995**, *243*, 222.

(4) Muenter, A. H.; DeZwaan, J. L.; Nathanson, G. M. *J. Phys. Chem. C* **2007**, *111*, 15043.

(5) Dempsey, L. P.; Brastad, S. M.; Nathanson, G. M. *J. Phys. Chem. Lett.* **2011**, *2*, 622.

(6) *Physical Properties of Glycerine and Its Solutions*; Glycerine Producers' Association: New York, 1963.

(7) Vargaftik, N. B.; Volkov, B. N.; Voljak, L. D. *J. Phys. Chem. Ref. Data* **1983**, *12*, 817.

(8) Archer, D. G.; Wang, P. *J. Phys. Chem. Ref. Data* **1990**, *19*, 371.

(9) Melander, W.; Horvath, C. *Arch. Biochem. Biophys.* **1977**, *183*, 200.

(10) Collins, K. D. *Proc. Natl. Acad. Sci.* **1995**, *92*, 5553.

(11) Baldwin, R. L. *Biophys. J.* **1996**, *71*, 2056.

(12) Collins, K. D. *Biophys. Chem.* **2006**, *119*, 271.

(13) Kherb, J.; Flores, S. C.; Cremer, P. S. *J. Phys. Chem. B* **2012**, *116*, 7389.

(14) Okur, H. I.; Kherb, J.; Cremer, P. S. *J. Am. Chem. Soc.* **2013**, *135*, 5062.

(15) Donaldson, D. J.; Vaida, V. *Chem. Rev.* **2006**, *106*, 1445.

(16) Tang, C. Y.; Allen, H. C. *J. Phys. Chem. A* **2009**, *113*, 7383.

(17) Bullock, T. H. O. R. G. A. *Introduction to nervous systems*; W.H. Freeman: San Francisco, 1977.

(18) Chung, S.-H.; Andersen, O. S.; Krishnamurthy, V. *Biological membrane ion channels dynamics, structure, and applications*; Springer: New York, 2007.

(19) Clausen, T. *Acta Physiologica* **2008**, *192*, 339.

(20) Aziz, E. F.; Ottosson, N.; Eisebitt, S.; Eberhardt, W.; Jagoda-Cwiklik, B.; Vacha, R.; Jungwirth, P.; Winter, B. *J. Phys. Chem. B* **2008**, *112*, 12567.

(21) Gurau, M. C.; Kim, G.; Lim, S. M.; Albertorio, F.; Fleisher, H. C.; Cremer, P. S. *Chemphyschem* **2003**, *4*, 1231.

(22) Heyda, J.; Pokorna, J.; Vrbka, L.; Vacha, R.; Jagoda-Cwiklik, B.; Konvalinka, J.; Jungwirth, P.; Vondrasek, J. *Phys. Chem. Chem. Phys.* **2009**, *11*, 7599.

(23) Jagoda-Cwiklik, B.; Vacha, R.; Lund, M.; Srebro, M.; Jungwirth, P. *J. Phys. Chem. B* **2007**, *111*, 14077.

(24) Le Calvez, E.; Blaudez, D.; Buffeteau, T.; Desbat, B. *Langmuir* **2001**, *17*, 670.

(25) Murdachaew, G.; Valiev, M.; Kathmann, S. M.; Wang, X. B. *J. Phys. Chem. A* **2012**, *116*, 2055.
(26) SimonKutscher, J.; Gericke, A.; Huhnerfuss, H. *Langmuir* **1996**, *12*, 1027.
(27) Tang, C. Y.; Huang, Z. S. A.; Allen, H. C. *J. Phys. Chem. B* **2010**, *114*, 17068.
(28) Uejio, J. S.; Schwartz, C. P.; Duffin, A. M.; Drisdell, W. S.; Cohen, R. C.; Saykally, R. J. *Proc. Natl. Acad. Sci.* **2008**, *105*, 6809.
(29) Vrbka, L.; Vondrasek, J.; Jagoda-Cwiklik, B.; Vacha, R.; Jungwirth, P. *Proc. Natl. Acad. Sci.* **2006**, *103*, 15440.
(30) Shen, Y. R.; Ostroverkhov, V. *Chem. Rev.* **2006**, *106*, 1140.
(31) Ji, N.; Ostroverkhov, V.; Tian, C. S.; Shen, Y. R. *Phys. Rev. Lett.* **2008**, *100*.
(32) Stiopkin, I. V.; Jayathilake, H. D.; Bordenyuk, A. N.; Benderskii, A. V. *J. Am. Chem. Soc.* **2008**, *130*, 2271.
(33) Nihonyanagi, S.; Yamaguchi, S.; Tahara, T. *J. Chem. Phys.* **2009**, *130*.
(34) Chen, X. K.; Hua, W.; Huang, Z. S.; Allen, H. C. *J. Am. Chem. Soc.* **2010**, *132*, 11336.
(35) Verreault, D.; Hua, W.; Allen, H. C. *J. Phys. Chem. Lett.* **2012**, *3*, 3012.
(36) Yamaguchi, S.; Tahara, T. *J. Chem. Phys.* **2008**, *129*.
(37) Allen, H. C.; Casillas-Ituarte, N. N.; Sierra-Hernandez, M. R.; Chen, X. K.; Tang, C. Y. *Phys. Chem. Chem. Phys.* **2009**, *11*, 5538.
(38) Hommel, E. L.; Ma, G.; Allen, H. C. *Anal. Sci.* **2001**, *17*, 1325.
(39) Ma, G.; Allen, H. C. *J. Phys. Chem. B* **2003**, *107*, 6343.
(40) Miner, C. S.; Dalton, N. N. *Glycerol*; Reinhold Pub. Corp.: New York, 1953.
(41) Silva, M. d. S.; Ferreira, P. C. *Glycerol : Production, Structure, and Applications*; Nova Science Publishers: New York, 2012.
(42) Champeney, D. C.; Joarder, R. N.; Dore, J. C. *Mol. Phys.* **1986**, *58*, 337.
(43) Root, L. J.; Stillinger, F. H. *J. Chem. Phys.* **1989**, *90*, 1200.
(44) Chelli, R.; Procacci, P.; Cardini, G.; Califano, S. *Phys. Chem. Chem. Phys.* **1999**, *1*, 879.
(45) Soltwisch, M.; Steffen, B. *Z. Naturfors. Sect. A-J. Phys. Sci.* **1981**, *36*, 1045.
(46) Kojima, S. *J. Mol. Struct.* **1993**, *294*, 193.
(47) Mendelovici, E.; Frost, R. L.; Kloprogge, T. *J. Raman. Spectrosc.* **2000**, *31*, 1121.
(48) Kataoka, Y.; Kitadai, N.; Hisatomi, O.; Nakashima, S. *Appl. Spectrosc.* **2011**, *65*, 436.
(49) Baldelli, S.; Schnitzer, C.; Shultz, M. J.; Campbell, D. J. *J. Phys. Chem. B* **1997**, *101*, 4607.
(50) Oh-e, M.; Yokoyama, H.; Baldelli, S. *Appl. Phys. Lett.* **2004**, *84*, 4965.
(51) Krebs, T.; Andersson, G.; Morgner, H. *Chem. Phys.* **2007**, *340*, 181.
(52) Okan, S. E.; Salmon, P. S. *J. Phys.-Condens. Matter* **1994**, *6*, 3839.
(53) Okan, S. E.; Salmon, P. S.; Champeney, D. C.; Petri, I. *Mol. Phys.* **1995**, *84*, 325.
(54) Muenter, A. H.; DeZwaan, J. L.; Nathanson, G. M. *J. Phys. Chem. B* **2006**, *110*, 4881.
(55) Brastad, S. M.; Albert, D. R.; Huang, M. W.; Nathanson, G. M. *J. Phys. Chem. A* **2009**, *113*, 7422.
(56) Dempsey, L. P.; Faust, J. A.; Nathanson, G. M. *J. Phys. Chem. B* **2012**, *116*, 12306.
(57) Jungwirth, P.; Tobias, D. J. *J. Phys. Chem. B* **2001**, *105*, 10468.

(58) Jungwirth, P.; Tobias, D. J. *J. Phys. Chem. B* **2002**, *106*, 6361.
(59) Liu, D. F.; Ma, G.; Levering, L. M.; Allen, H. C. *J. Phys. Chem. B* **2004**, *108*, 2252.
(60) Schnitzer, C.; Baldelli, S.; Shultz, M. J. *J. Phys. Chem. B* **2000**, *104*, 585.
(61) Raymond, E. A.; Richmond, G. L. *J. Phys. Chem. B* **2004**, *108*, 5051.
(62) Tian, C. S.; Ji, N.; Waychunas, G. A.; Shen, Y. R. *J. Am. Chem. Soc.* **2008**, *130*, 13033.
(63) Bian, H. T.; Feng, R. R.; Xu, Y. Y.; Guo, Y.; Wang, H. F. *Phys. Chem. Chem. Phys.* **2008**, *10*, 4920.
(64) Adamson, A. W.; Gast, A. P. *Physical Chemistry of Surfaces*; Wiley: New York, 1997.
(65) Watry, M. R.; Tarbuck, T. L.; Richmond, G. I. *J. Phys. Chem. B* **2003**, *107*, 512.
(66) Sovago, M.; Campen, R. K.; Bakker, H. J.; Bonn, M. *Chem. Phys. Lett.* **2009**, *470*, 7.
(67) Tang, C. Y.; Huang, Z. S.; Allen, H. C. *J. Phys. Chem. B* **2011**, *115*, 34.
(68) Pieniazek, P. A.; Tainter, C. J.; Skinner, J. L. *J. Am. Chem. Soc.* **2011**, *133*, 10360.
(69) Casillas-Ituarte, N. N.; Callahan, K. M.; Tang, C. Y.; Chen, X. K.; Roeselova, M.; Tobias, D. J.; Allen, H. C. *Proc. Natl. Acad. Sci.* **2010**, *107*, 6616.
(70) Ishiyama, T.; Morita, A. *J. Phys. Chem. C* **2007**, *111*, 738.
(71) Ishiyama, T.; Morita, A. *J. Chem. Phys.* **2009**, *131*.
(72) Ishiyama, T.; Morita, A. *J. Phys. Chem. C* **2009**, *113*, 16299.
(73) Tian, C. S.; Shen, Y. R. *Chem. Phys. Lett.* **2009**, *470*, 1.
(74) Sovago, M.; Campen, R. K.; Wurpel, G. W. H.; Mueller, M.; Bakker, H. J.; Bonn, M. *Phys. Rev. Lett.* **2008**, *101*.
(75) Sovago, M.; Campen, R. K.; Wurpel, G. W. H.; Muller, M.; Bakker, H. J.; Bonn, M. *Phys. Rev. Lett.* **2008**, *100*.
(76) Wei, X.; Miranda, P. B.; Zhang, C.; Shen, Y. R. *Physical Review B* **2002**, *66*.
(77) Du, Q.; Freysz, E.; Shen, Y. R. *Science* **1994**, *264*, 826.
(78) Benjamin, I.; Wilson, M.; Pohorille, A. *The Journal of Chemical Physics* **1994**, *100*, 6500.
(79) Stanners, C. D.; Du, Q.; Chin, R. P.; Cremer, P.; Somorjai, G. A.; Shen, Y. R. *Chem. Phys. Lett.* **1995**, *232*, 407.
(80) Shen, Y. R. *The Principles of Nonlinear Optics*; J. Wiley: New York, 1984.
(81) Shen, Y. R. *Nature* **1989**, *337*, 519.
(82) Uchino, T.; Yoko, T. *Science* **1996**, *273*, 480.
(83) Ju, S. S.; Wu, T. D.; Yeh, Y. L.; Wei, T. H.; Huang, J. Y.; Lin, S. H. *J. Chin. Chem. Soc.* **2001**, *48*, 625.
(84) Mudalige, A.; Pemberton, J. E. *Vib. Spectrosc* **2007**, *45*, 27.
(85) Hidaka, F.; Yoshimura, Y.; Kanno, H. *J. Solution Chem.* **2003**, *32*, 239.
(86) Smith, J. D.; Saykally, R. J.; Geissler, P. L. *J. Am. Chem. Soc.* **2007**, *129*, 13847.
(87) Sharpe, A. G. *J. Chem. Educ.* **1990**, *67*, 309.
(88) Hua, W.; Chen, X. K.; Allen, H. C. *J. Phys. Chem. A* **2011**, *115*, 6233.
(89) Hua, W.; Jubb, A. M.; Allen, H. C. *J. Phys. Chem. Lett.* **2011**, *2*, 2515.
(90) Tian, C. S.; Byrnes, S. J.; Han, H. L.; Shen, Y. R. *J. Phys. Chem. Lett.* **2011**, *2*, 1946.
(91) Cwiklik, L.; Andersson, G.; Dang, L. X.; Jungwirth, P. *Chemphyschem* **2007**, *8*, 1457.

(92) Pegram, L. M.; Record, M. T. *Proc. Natl. Acad. Sci.* **2006**, *103*, 14278.
(93) Pieniazek, P. A.; Tainter, C. J.; Skinner, J. L. *J. Chem. Phys.* **2011**, *135*.
(94) Nihonyanagi, S.; Ishiyama, T.; Lee, T.; Yamaguchi, S.; Bonn, M.; Morita, A.; Tahara, T. *J. Am. Chem. Soc.* **2011**, *133*, 16875.
(95) Darnell, J. E.; Lodish, H. F.; Baltimore, D. *Molecular cell biology*; Scientific American Books : Distributed by W.H. Freeman: New York, 1990.
(96) Jorgensen, P. L. *Physiological Reviews* **1980**, *60*, 864.
(97) Scheiner-Bobis, G. *Eur. J. Biochem.* **2002**, *269*, 2424.
(98) Spanswick, R. M. *Annual Review of Plant Physiology and Plant Molecular Biology* **1981**, *32*, 267.
(99) Collins, K. D.; Neilson, G. W.; Enderby, J. E. *Biophys. Chem.* **2007**, *128*, 95.
(100) Hajari, T.; Ganguly, P.; van der Vegt, N. F. A. *J. Chem. Theory Comput.* **2012**, *8*, 3804.
(101) Hess, B.; van der Vegt, N. F. A. *Proc. Natl. Acad. Sci.* **2009**, *106*, 13296.
(102) Hua, W.; Verreault, D.; Adams, E. M.; Huang, Z.; Allen, H. C. *Submitted* **2013**.
(103) Finlayson, A. C. *J. Chem. Educ.* **1992**, *69*, 559.
(104) Sovago, M.; Vartiainen, E.; Bonn, M. *J. Chem. Phys.* **2009**, *131*.
(105) Sovago, M.; Wurpel, G. W. H.; Smits, M.; Muller, M.; Bonn, M. *J. Am. Chem. Soc.* **2007**, *129*, 11079.
(106) Gershevitz, O.; Sukenik, C. N. *J. Am. Chem. Soc.* **2004**, *126*, 482.
(107) Gomez-Fernandez, J. C.; Villalain, J. *Chem. Phys. Lipids* **1998**, *96*, 41.
(108) Miranda, P. B.; Du, Q.; Shen, Y. R. *Chem. Phys. Lett.* **1998**, *286*, 1.
(109) Gericke, A.; Huhnerfuss, H. *Thin Solid Films* **1994**, *245*, 74.
(110) Sakai, H.; Umemura, J. *Colloid. Polym. Sci.* **2008**, *286*, 1637.
(111) Ma, G.; Allen, H. C. *Langmuir* **2006**, *22*, 5341.
(112) Richmond, G. L. *Chem. Rev.* **2002**, *102*, 2693.
(113) Shultz, M. J.; Baldelli, S.; Schnitzer, C.; Simonelli, D. *J. Phys. Chem. B* **2002**, *106*, 5313.
(114) Bonn, M.; Bakker, H. J.; Tong, Y. J.; Backus, E. H. G. *Biointerphases* **2012**, *7*.
(115) Jubb, A. M.; Hua, W.; Allen, H. C. In *Annual Review of Physical Chemistry, Vol 63*; Johnson, M. A., Martinez, T. J., Eds.; Annual Reviews: Palo Alto, 2012; Vol. 63, p 107.
(116) Nihonyanagi, S.; Yamaguchi, S.; Tahara, T. *J. Am. Chem. Soc.* **2010**, *132*, 6867.